CrystEngComm

Accepted Manuscript

ROYAL SOCIETY OF CHEMISTRY

www.rsc.org/crystengcomm

Graphical abstract:

In cyclic alpha-peptoids inter-annular CH•••OC hydrogen bonds provide face to face or side by side arrangement of macrocycles mimicking beta-sheet secondary structure in proteins.
Side chains may promote the formation of peptoids nanotubes, acting as pillars among neighbouring macrocycles.

Cite this: DOI: 10.1039/c0xx00000x

www.rsc.org/xxxxxx

ARTICLE TYPE

Solid state assembly of cyclic α-peptoids

Consiglia Tedesco,*[a,b] Loredana Erra,[a] Irene Izzo[a] and Francesco De Riccardis[a]

Received (in XXX, XXX) Xth XXXXXXXXX 20XX, Accepted Xth XXXXXXXXX 20XX
DOI: 10.1039/b000000x

The solid state assembly of free and metal coordinated cyclic α-peptoids has been examined with the aim to find common underlying features and to direct the design of new functional biomimetic materials with desired properties in terms of molecular recognition, drug-delivery and catalysis. The lack of the amide proton prevents the formation of NH···OC hydrogen bonds and weaker interactions play a key role in the intermolecular recognition and assembly. Inter-annular CH···OC hydrogen bonds provide face to face or side by side arrangement of macrocycles in a way that can be considered the peptoid counterpart of β-sheet secondary structure in proteins. The choice of side chains is crucial for the solid state properties of α-cyclic peptoids. Side chains have a strong influence on the solid state assembly of peptoid macrocycles: they may provide competing interactions to CH···OC inter-annular hydrogen bonds, leading either to a *T*-shape or to a tubular arrangement of the peptoid macrocycles. The size of the macrocycle is another important factor influencing the tubular arrangement. In particular, a bigger size of the macrocycle promotes side by side respect to *T*-shape interactions. Hirshfeld surfaces and their fingerprint analysis allowed to analyze the contributions of weak intermolecular interactions, as weak CH···OC hydrogen bonds and CH-pi interactions, towards the crystal packing.

Dedicated to Prof. Emeritus Adolfo Zambelli on occasion of his 80th birthday, "for a tree is recognized by its fruit".

Introduction

Natural and synthetic macrocycles are the subject of an intense and continuous research activity in many areas as biochemistry, crystal engineering, supramolecular chemistry, catalysis and material sciences. Research groups were able to exploit their biological and recognition properties, providing imaginative connections among their graceful structures and remarkable functions.[1]

Cyclic peptoids belong to the realm of macrocyclic compounds and, for their biostability and potential diversity, are useful building blocks for the construction of attractive supramolecular architectures with novel chemical properties and defined biological activities.

Peptoids differ from peptides for the side chains position, which is shifted by one position along the peptide backbone to give *N*-substituted oligoglycines (Fig. 1).[2] Their functional groups variousness, coupled with simple chemical synthesis, makes them highly desirable bioinspired materials, as Zuckermann pointed out in a recent review.[3]

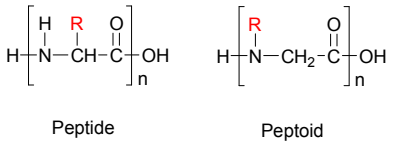

Fig. 1 Comparison between peptide and peptoid structures.

The side-chain C→N atom shift abolishes the α-carbon stereogenic centres and generates an achiral backbone. The lack of the amide protons prevents the formation of hydrogen-bond networks, but does not hamper the formation of helical or ribbon secondary structures.[4] Moreover, the almost isoenergetic tertiary amide bond *cis*/*trans* conformations, adds further flexibility to the peptoid backbone (when compared to the corresponding peptides, Fig. 2).

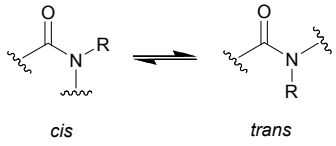

Fig. 2 *Cis*/*trans* conformational isomerism in tertiary amides.

The cyclization of linear oligomers represents a useful strategy to induce conformational rigidity and enlightening contributions demonstrate that cyclic peptoids encode reverse-turn type secondary structures.[5] Cyclic peptoids are interesting scaffolds to work with for three main reasons: i) their ample chemical diversity (gained either by tailoring the size of the macrocycle or by proper functional side groups selection); ii) their structural ordering; iii) their controlled flexibility.

It has been demonstrated that cyclic peptoids promote the transport across a phospholipid membrane, probably via a carrier mechanism[6] and for this reason they may represent new motifs on which to base artificial ionophoric antibiotics. The biological assays indicated in some cases antifungal activity and no toxicity toward red blood cells.[7] A cyclic conjugate containing ethisterone ligands modulates the activity of the androgen receptor, showing potent antiproliferative activity in LNCaP-abl cells, a model of therapy-resistant prostate cancer.[8] Moreover due to their nature of bioinspired polymers they show a great potential in the materials chemistry.[9] For their

high affinity to metal cations they have been tested also as phase transfer catalysts (with performances comparable to crown ethers) and as powerful ligands for the gadolinium ion.[10] Cyclic *N*-substituted glycines have been characterized by several techniques, NMR being the prevailing one.[11] Interestingly, the first rigorous structural studies date back to the early 70's and report the X-ray crystallographic investigation on the cyclic oligopeptides of sarcosine (*N*-methylglycine).[12] Almost forty years later, in 2007, Kirshenbaum and his group published the first high-resolution structures of cyclic peptoid hetero-oligomers[5b] and soon after our group provided the first X-ray crystal structure of a cyclic peptoid coordinated to a metal ion.[13] Recently Kirshenbaum demonstrated that a highly thermostable peptoid cyclo-octamer can reversibly uptake and release water molecules from its inner cavity in a single-crystal-to-single-crystal transformation.[14] We also probed the attitude of chelating *N*-methoxyethyl glycine residues (included in cyclic hexapeptoid scaffolds) to trigger the formation of a *1D* coordination polymer.[15] Here we wish to present a survey of the solid state assembly of free and metal coordinated cyclic α-peptoids[16] with the aim to find common underlying features and to direct the design of new functional biomimetic materials with desired properties in terms of molecular recognition, drug-delivery, catalysis, and other critical area of modern chemistry. In this contribution we also report the X-ray crystal structure of the newly synthesized cyclotetra-*N*-benzylglycine (cyclo-(Npm)$_4$, 5 in Table 1 and Figure 7).

Table 1 Sequence of *cis* (*c*) and *trans* (*t*) conformation of amide groups in the X-ray molecular structures of cyclic peptoids.

N. of residues	Sequence	Peptoid name	Notes	Ref.
3	*ccc*	cyclo-(Sar)$_3$ (**1**)		20
	ccc	cyclo-(Nal)$_3$ (**2**)		21
4	*ctct*	cyclo-(Sar)$_4$ (**3**)		12
	ctct	cyclo-(Nbe)$_4$ (**4**)		13
	ctct	cyclo-(Npm)$_4$ (**5**)		This work
5	*ccctt*	cyclo-(Sar)$_5$ (**6**)	*a*	25
6	*cctcct*	cyclo-(Sar)$_6$ (**7**)	*b*	26
	cctcct	cyclo-(Npm-Nme)$_3$ (**8**)	*b*	5b
	cctcct	cyclo-(Nspe-Nspe-Nph)$_2$ (**9**)		27
	cctcct	cyclo-(Nme)$_6$ (**10**)		15
	cctcct	cyclo-(Npm$_2$-Nph-Npm$_2$-Nnp) (**11**)		28
	all *trans*	cyclo-(Nme)$_6$ Na complex (**10**·Na^+)		15
	all-*trans*	cyclo-(Nbe)$_6$ Sr complex (**12**·Sr^{2+})		13
7	*cccctttt*	cyclo-(Sar)$_7$ (**13**)	*a*	30
8	*ccttcctt*	cyclo-(Sar)$_8$ (**14**)	*a*	31
	ccttcctt	cyclo-(Npm-Nme)$_4$ (**15**)		5b
	ccttcctt	cyclo-(Npa-Nme-Nph-Nph)$_2$ (**16**)	*c*	14
9	*ccccctcct*	cyclo-(Nspe)$_9$ (**17**)	*d*	32
10	*ccctttcctt*	cyclo-(Sar)$_{10}$ (**18**)	*b*	33

[a] hydrate form, [b] methanol solvate, [c] both anhydrous and hydrate form, [d] ethanol solvate

List of abbreviations: Sar = sarcosine, Nal = *N*-(allyl)glycine, Nnp = *N*-(naphthyl)glycine, Nbe = *N*-(benzyloxyethyl)glycine, Npm = *N*-(benzyl)glycine, Nme = *N*-(methoxyethyl)glycine, Nph = *N*-(phenyl)glycine, Npa = *N*-(propargyl)glycine, Nspe = (S)-*N*-(1-phenylethyl)glycine.

Results and discussion

In this work we will recapitulate the main structural traits of cyclic *N*-substituted glycines on the basis of their crystal structures with particular attention to the role of weak intermolecular interactions, as weak hydrogen bonds[17] (CH···CO, CH-pi interactions) or pi-pi interactions.[18] Hirshfeld fingerprint analysis has been used to study the nature of interactions and their quantitative contributions towards the crystal packing.[19]

The examined α-cyclopeptoids have been grouped on the basis of the ring size, starting from three and concluding with ten residues in the macrocycle

Table 1 provides a list of the examined cyclic α-peptoids, together with their *cis* (*c*) and *trans* (*t*) amide bonds conformations.

Trimeric cyclic peptoids

The close examination of the cyclic α-peptoid crystal structures starts with the simplest macrocycles: the cyclotrisarcosyl**,** cyclo-(Sar)$_3$ (**1**),[20] and the *N*,*N*′,*N*″-triallyl-*cyclo*-triglycine, cyclo-(Nal)$_3$ (**2**, Fig. 3).[21]

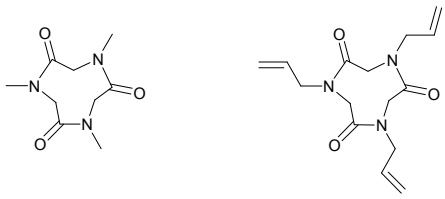

Fig. 3 Trimeric cyclic peptoids **1** and **2** studied by X-ray analysis.

Both those nine-membered ring molecules show a *ccc* sequence of the amide bonds and a C_3-symmetric "crown" conformation. By analogy with calixarenes, the intra-annular methylene groups define the lower rim of the crown, while the side chains, together with the oxygen atoms of the carbonyls, define the upper rim.[21]

Compounds **1** and **2** crystallize with two crystallographically independent molecules in the unit cell. In both the cases these two molecules interact by means of weak CH···OC hydrogen bonds, where the CH belong to the intra-annular methylene groups (Fig. 4).

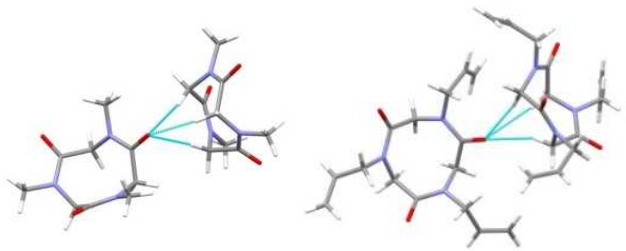

Fig.4 *T*-shaped arrangement of the two independent molecules in a) cyclo-(Sar)$_3$ (**1**), and b) cyclo-(Nal)$_3$ (**2**).

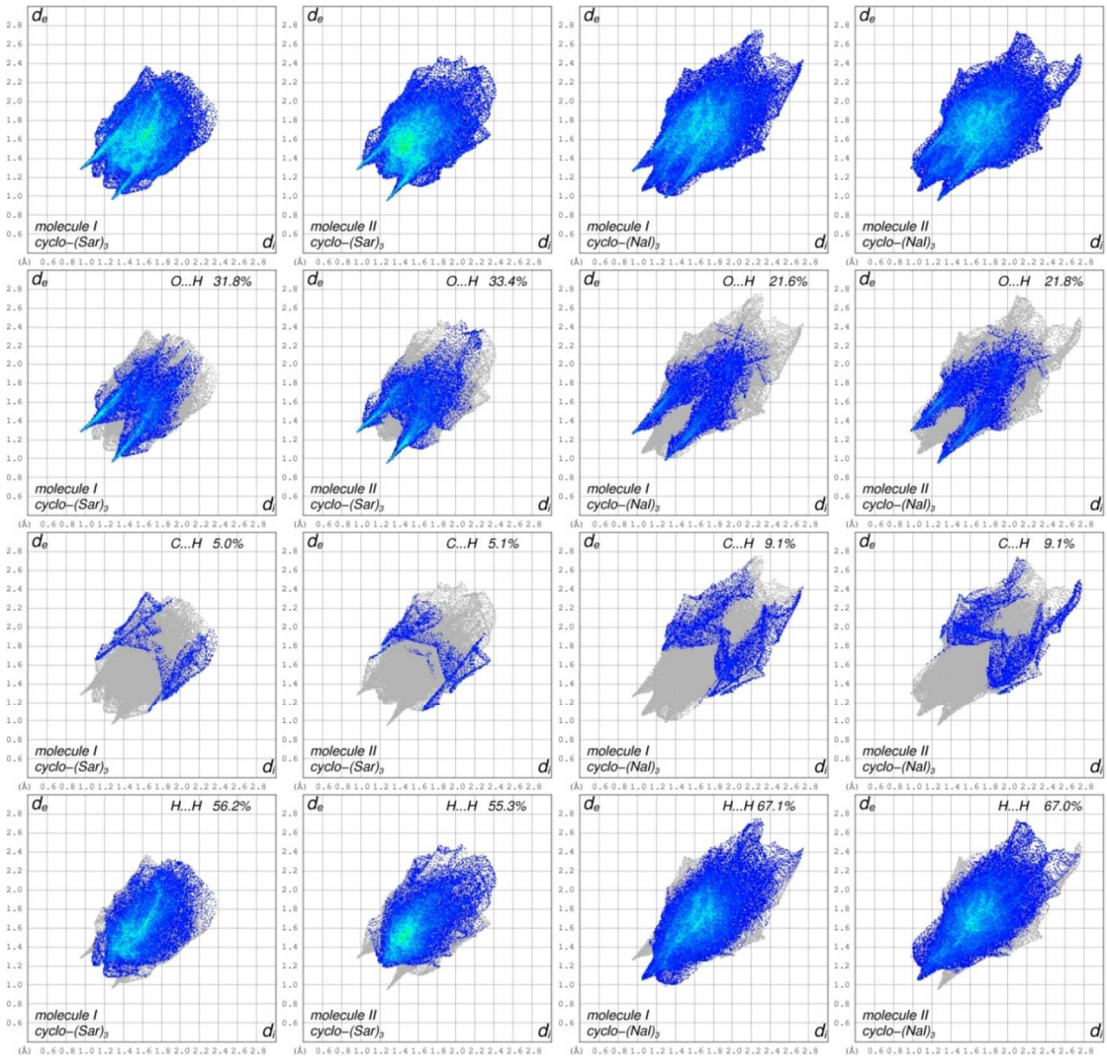

Fig. 5 Comparison of full fingerprint plots and decomposed fingerprint plots into O···H, C···H and H···H intermolecular interactions of the two independent molecules (I and II) respectively for cyclo-$(Sar)_3$ (**1**) and cyclo-$(NaI)_3$ (**2**).

This arrangement will be termed *T*-shape interaction, where the two interacting molecules are almost perpendicular to each other. It is shown in Fig. 4 for cyclo-$(Sar)_3$ (**1**) and cyclo-$(NaI)_3$ (**2**). The angle between the least-squares planes defined by peptoid backbone atoms is 62.6° for **1** and 63.7° for **2**. It represents one of the possible ways for two cyclopeptoid molecules to interact with each other via hydrogen bonds. This peculiar arrangement will again be encountered in the following sections.

As there are two independent molecules in the asymmetric unit (Z'=2), two Hirshfeld fingerprint plots are provided for each independent molecule in Fig 5.

At a first glance it is evident that a much narrower plot is obtained in the case of cyclo-$(Sar)_3$ (**1**) with d_i and d_e values ranging from 1.0 Å to 2.4 Å, while in the case of cyclo-$(NaI)_3$ (**2**) d_i and d_e values extend up to 2.8 Å. Thus, it can be concluded that cyclo-$(Sar)_3$ crystals are more efficiently packed than cyclo-$(NaI)_3$.The fingerprint plots in Fig. 5 result to be rather unsymmetrical (in particular for compound **2**), a closer inspection reveals that, for both compounds **1** and **2,** the features at the upper left of the fingerprint plot for molecule I are identically reproduced in the lower right of the fingerprint plot for molecule II and vice versa. This means that molecule I acts as hydrogen bond donor and molecule II constitutes the acceptor counterpart and vice versa. As for cyclo-$(Sar)_3$ (**1**) short green-blue spikes appears, corresponding to CO··· CH contacts (the shortest at 2.25 Å). As for cyclo-$(NaI)_3$ (**2**) green-blue streaks almost disappear and the spikes markedly broaden, in fact in compound **2** all three CO groups of each independent molecule are involved in O···H contacts with distances ranging from 2.28 Å to 2.58 Å and two CO groups accept respectively three and two hydrogen bonds. As for the region for C···H contacts in the case of cyclo-$(NaI)_3$ (**2**) the characteristic wings of CH-pi interactions are not much evident, indicating that they do not play a key role in the crystal packing. The rest of the plot for both compounds **1** and **2** is largely determined by H···H contacts, while compound **1** does not show very close H···H

contacts (the shortest being at 2.30 Å), for compound **2** close H···H contacts (down to 2.11 Å) are observed.

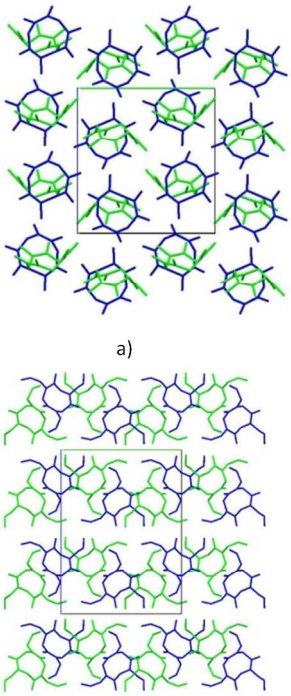

Fig. 6 a) Alternated layers of independent molecules in the crystal packing of a) cyclo-$(Sar)_3$ (**1**) and b) cyclo-$(Nal)_3$ (**2**) as viewed along the *a* axis. Hydrogen atoms have been omitted for clarity.

In both the cases, the crystal packing is characterized by alternated layers of independent molecules with an up/down arrangement similar to that observed in calixarenes (Fig. 6).[22]

Tetrameric cyclic peptoids

With regards to tetrameric cyclic peptoids, two X-ray crystal structures are already known: one belongs to the cyclotetrasarcosyl, cyclo-$(Sar)_4$ (**3**),[12] and the other one is related to the cyclotetra-*N*-benzyloxyethylglycine, cyclo-$(Nbe)_4$ (**4**).[13] A third one is presented for the first time in this work and pertains to the cyclotetra-*N*-benzylglycine, cyclo-$(Npm)_4$ (**5**, Fig. 7).

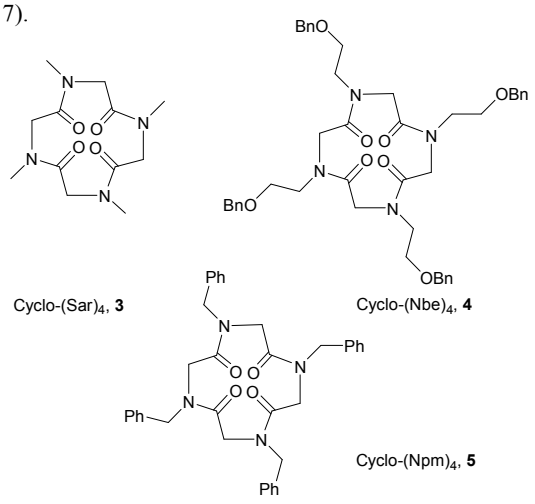

Fig. 7 Tetrameric cyclic peptoids **3**-**5** studied by X-ray analysis.

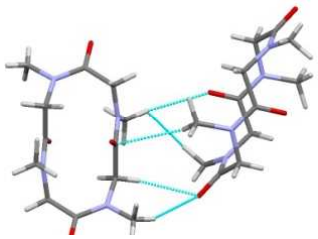

Fig. 8 *T*-shaped arrangement of two adjacent molecules in the crystal structures of cyclo-$(Sar)_4$ (**3**), short distance molecular interactions are shown in light-blue.

In all three cases the X-ray molecular structure showed a *ctct* tetralactam core geometry and overall rectangular shape of the peptoid backbone. The molecular inversion centre is preserved in all crystal structures.

For the cyclo-$(Sar)_4$ (**3**) the predominant intermolecular interactions are very weak CH···OC hydrogen bonds between methyl hydrogen atoms of the side chains and the carbonyl oxygen atoms. These interactions are responsible for a *T*-shaped arrangement of neighbouring peptoid molecules (Fig. 8), with the angle between the peptoid backbone least-squares planes of 82.80°.

The overall arrangement of the molecules in the crystal is best viewed along [011] direction (Fig. 9).

In the corresponding Hirshfeld fingerprint plot (Fig. 10) two symmetrical green-blue streaks appear at the upper left and bottom right, starting at d_i+d_e~2.5 Å, corresponding to CH···OC contacts. The characteristic spikes of hydrogen bonds are not present, indicating the absence of close CH···OC contacts (the shortest at 2.46 Å), which are nevertheless highly directional and numerous. The rest of the plot is determined by H···H contacts (the shortest at 2.24 Å) with the majority of points in the d_i/d_e range between 1.2 Å and 2.0 Å and a central green-blue streak (around d_i+d_e~2.8 Å) corresponding to H···H contacts among methyl groups.

It can be concluded that methyl groups prevent the tight stacking of the cyclopeptoid molecules on top of each others, favouring a *T*-shaped arrangement of neighbour peptoid molecules.

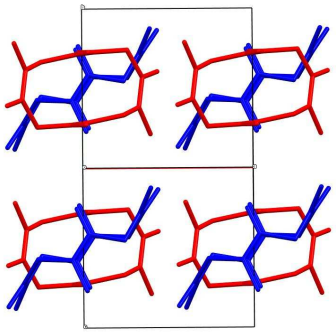

Fig.9 Crystal packing of cyclo-$(Sar)_4$ (**3**) as viewed along the [011] direction. Red and blue colours highlight molecules showing a *T*-shape interaction. Hydrogen atoms have been omitted for clarity.

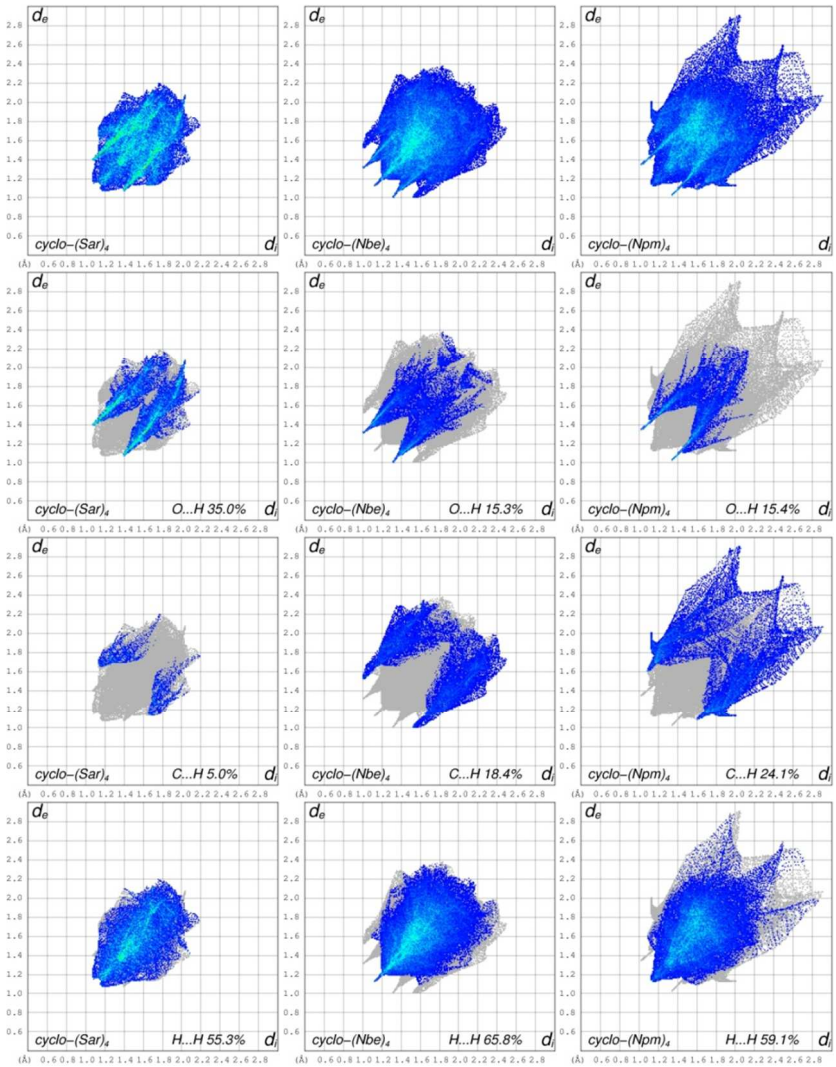

Fig. 10 Comparison of full fingerprint plots and decomposed fingerprint plots into O···H, C···H and H···H intermolecular interactions respectively for cyclo-(Sar)$_4$ (**3**), cyclo-(Nbe)$_4$ (**4**) and cyclo-(Npm)$_4$ (**5**).

In the case of the cyclo-(Nbe)$_4$ (**4**) the side chains fold outside the plane of the macrocycle, inducing an overall flat disc shape of the molecule (Fig. 11a). Evaluation of the crystal packing evidences that the molecules stack along the shortest cell axis, which is the *b* axis, to form nanotubes in a very similar way to that observed for peptide nanotubes (Fig. 11c,d).[23] While in the case of alternate D-L peptides NH···OC hydrogen bonds connect the peptides, in the case of cyclic tetrapeptoids weak CH···OC hydrogen bonds provide extended intermolecular contacts (Fig. 11c and d). The shortest contacts involve two methylene hydrogen atoms and two *trans* carbonyl oxygen atoms, which are almost perpendicular to the plane of the ring (shortest contacts are: CH_2···OC 2.31 Å, CO···OC 2.928(3) Å). This could be described as the first example of β-sheet like peptoid secondary structure, where each ring stacks on top of each other by means of CH···OC hydrogen bonds.

The aromatic side chains in **4** contribute to stabilize the peptoid nanotube by establishing CH_{ar}···O interactions and CH_2-pi interactions between stacked macrocycles (shortest contacts are CH_{ar}···O 2.59 Å and CH_2···C_{ar}2.79 Å).

Intertubular contacts are established through side-by-side CH_2···OC hydrogen bonds (at 2.49 Å distance) and CH_{ar}-pi interactions of the aromatic moieties (contacts at 2.52 Å and 2.70 Å).

Hirshfeld fingerprint for compound **4** (Fig. 10) occupies a larger region of the plot with respect to **3**, with d_i and d_e values ranging from 1.0 Å to 2.5 Å. It is characterized by: i) two symmetric and very sharp features for CH_2···OC hydrogen bonds, corresponding to intratubular hydrogen bonds at a distance of 2.31 Å; ii) two symmetric green-blue streaks, starting at d_i+d_e= 2.5 Å, corresponding to intertubular CH_2···OC hydrogen bonds; ii) two wings at the upper left and bottom right of the plot, typical of CH-pi interactions, approaching 2.5 Å; iii) a central green-blue spike for H···H contacts, the closest one being at 2.25 Å between the aromatic moieties of adjacent nanotubes.

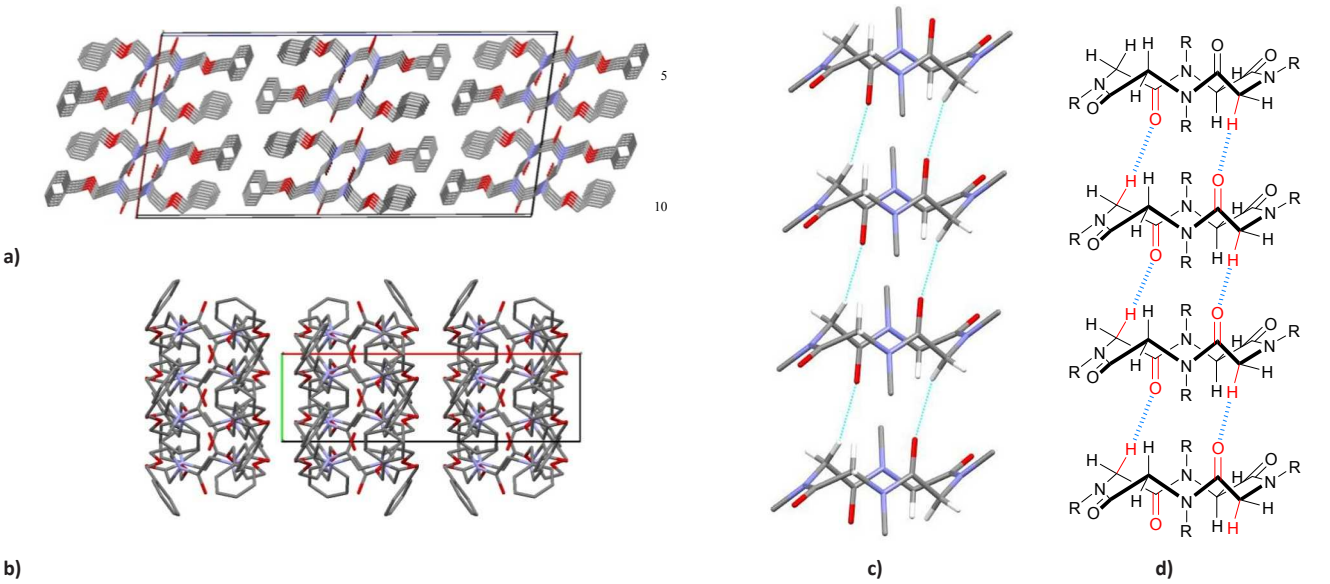

Fig. 11 a) and b) Crystal packing of cyclo-$(Nbe)_4$ (**4**) respectively along *b*, *c* axes, hydrogen atoms have been omitted for clarity. c) and d) Network of CO···HC interactions inducing the tubular arrangement of peptoid nanotubes. Benzyloxyethyl moieties and hydrogen atoms have been omitted for clarity.

The X-ray crystal structure of cyclo-$(Npm)_4$ (**5**) allows to better clarify the importance of the side chains in the solid state arrangement of the molecular units.

Superimposition of the X-ray molecular structures of cyclo-$(Nbe)_4$ (**4**) and cyclo-$(Npm)_4$ (**5**) shows that the backbone conformation of the two cyclic compounds is almost identical. The only difference lies in the conformation adopted by the side groups: in particular, in the case of cyclo-$(Nbe)_4$ (**4**) the values for $\chi 1$ angles[24] are respectively -82° and 87°, while in the case of the cyclo-$(Npm)_4$ (**5**) those values are -102° and -66° (Fig. 12).

Benzyl side chains provide intermolecular contacts with backbone carbonyl groups by means of CH_{ar}···OC hydrogen bonds (at 2.36 Å) and CH_2-pi interactions (CH_2-C_{ar} distances 2.78 Å and 2.88 Å). As depicted in Fig. 13a, a *T*-shaped arrangement of neighbouring molecules is determined, with an angle between the peptoid ring least-squares planes of 86.6°.

CH_{ar}-pi interactions between side chains contribute to further stabilize this arrangement (the shortest CH_{ar}-C_{ar} distance is 2.69 Å, see Fig. 13b).

The overall arrangement of the molecules in the crystal is best viewed along [110] direction (Fig. 14).

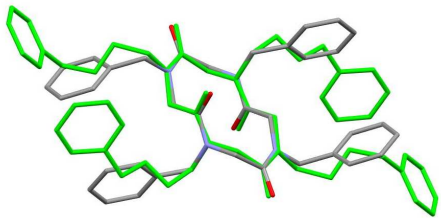

Fig. 12 X-ray molecular structures of cyclo-$(Nbe)_4$ (**4**, in green colour) and cyclo-$(Npm)_4$ (**5**). Hydrogen atoms have been omitted for clarity.

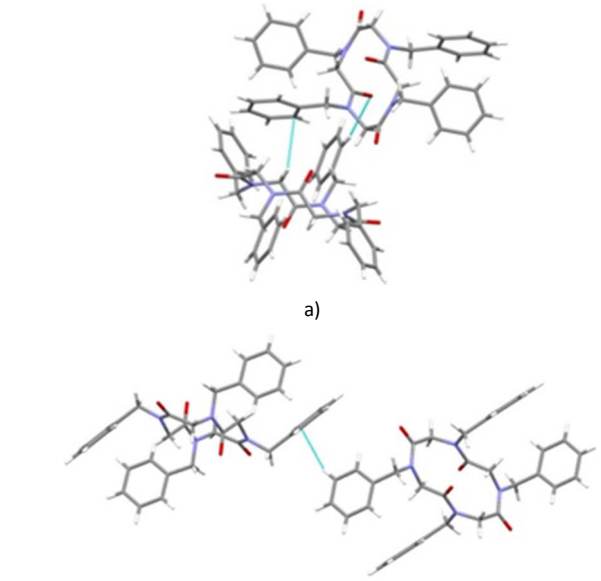

Fig. 13 *T*-shaped arrangement of adjacent molecules in the crystal structures of cyclo-$(Npm)_4$ (**5**): a) CH_{ar}···OC hydrogen bonds and CH_2-pi interactions; b) CH_{ar}-pi interactions among side chains.

Hirshfeld fingerprint plot for compound **5** in Fig. 10 occupies an even larger region with respect to compounds **3** and **4** of the plot with d_i and d_e values ranging from 1.0 Å to 2.85 Å.

Two symmetric sharp blue-green spikes correspond to CH···OC contacts (Fig. 13a). The wings at the upper left and bottom right of the plot are indicative of CH_2-pi and CH_{ar}-pi interactions (Fig 13a and 13b); the former is almost superimposed to O···H contacts, the latter has a rather defined shape, which recalls the fingerprint plot of benzene. [19b,c]

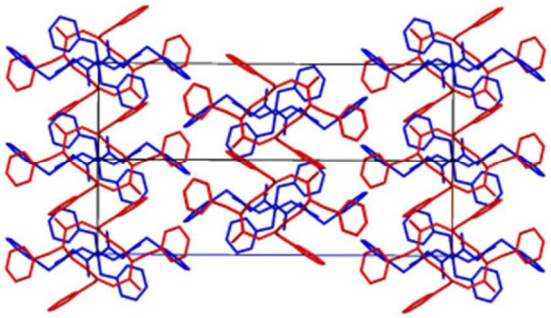

Fig. 14 Crystal packing of cyclo-(Npm)$_4$ (**5**) as viewed along [110] direction, different colors highlight the *T*-shaped arrangement of molecules in the crystal. Hydrogen atoms have been omitted for clarity.

The central green-blue region is determined by H···H contacts, whose closest contacts are at 2.27 Å. The long and sparse blue region is determined by longer contacts, which indicate a less dense packing for **5.**

As in the case of cyclo-(Sar)$_4$ (**3**, see Fig. 9), the side chains prevent the tight stacking of the cyclopeptoid molecules on top of each other, hampering the inter-annular backbone atoms interactions and favouring a *T*-shaped arrangement of neighbouring peptoid molecules.

Thus, tubular arrangement is realized because the backbone atoms interact with backbone atoms and side chain atoms with side chain atoms. This observation highlights the fact that, independently from the backbone conformation, the side chains are able to stabilize or prevent a tubular arrangement.

Pentameric cyclic peptoids

Only one crystal structure is known for pentameric cyclic peptoids: it is the dihydrate form of cyclopentasarcosyl, cyclo-(Sar)$_5$ (**6**, Fig. 15).[25]

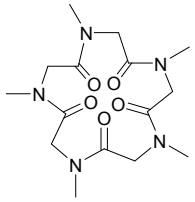

Cyclo-(Sar)$_5$, **6**

Fig. 15 Pentameric cyclic peptoid **6** studied by X-ray crystallography.

As listed in Table 1, the backbone amide bonds *cis*/*trans* sequence is: *ccctt*. Each cyclopeptoid molecule binds to two water molecules by means of hydrogen bonds involving two carbonyl groups (CO···OH distances are 2.740 Å and 2.746 Å). Water molecules cluster into square-planar tetramers and each water molecule binds to a cyclopeptoid molecule forming a ribbon, which runs parallel to the *a* axis (Fig. 16a and 16b). The central part of this supramolecular ribbon is made by water tetramers and the edges by the cyclopeptoid molecules.

The crystal packing can be described as a herringbone arrangement of ribbons, with a wet core and dry edges (Fig. 16c). Molecules at the dry edges are in a *T*-shaped arrangement by means of CH···OC hydrogen bonds, the angle between the least-squares planes defined by peptoid backbone atoms of adjacent molecules is 65.58°.

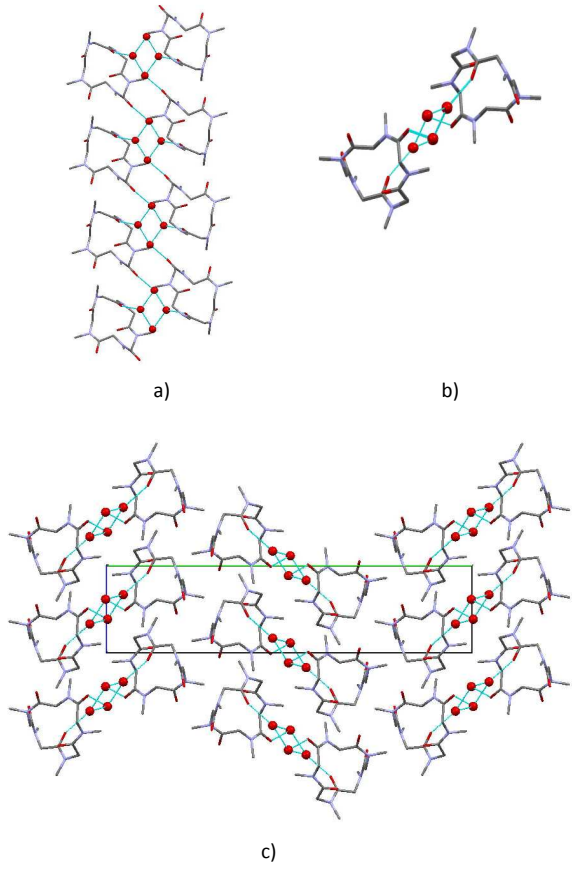

Fig. 16 a) Cyclo-(Sar)$_5$ (**6**) and water molecules form a supramolecular ribbon, which extends along the *a* axis; b) top view of the ribbon as viewed along the a axis; c) crystal packing of cyclo-(Sar)$_5$ (**6**) as viewed along the *a* axis. Supramolecular ribbons pack in a herringbone arrangement. Hydrogen atoms have been omitted for clarity.

Fig. 17 displays the Hirshfeld fingerprint plots for the hydrate form of cyclo-(Sar)$_5$ (**6**), the plot refers to the molecule of cyclo-(Sar)$_5$ (**6**) and, since water molecule hydrogen atoms were not located, their contribution does not appear in the plot, which results to have a rather symmetrical shape.

A closer inspection reveals that: i) the upper left hydrogen spike has a more evident central green-blue streak than the lower right spike, which accounts for CH···O hydrogen bonds, where the oxygen atom belong to water molecules; ii) there is a central green streak starting at (d_i,d_e) = (1.35 Å,1.35 Å) corresponding to O···O contacts.

Close H··· H head to head contacts down to 2.24 Å are observed, which correspond to contacts among hydrogen atoms belonging to methyl groups facing at the dry edges

The plot extends up to 2.5 Å in both directions, indicating a non-optimally dense packing.

In this case the crystal packing is strongly influenced by the presence of water molecules, which bridge the backbone carbonyl groups, preventing any possible tight stacking among the macrocycles.

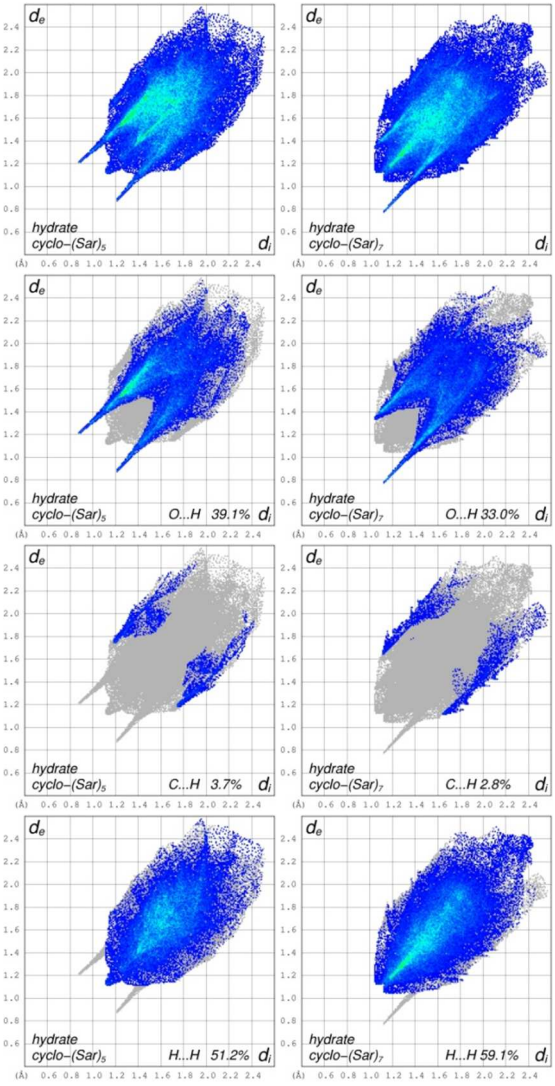

Fig. 17 Comparison of full fingerprint plots and decomposed fingerprint plots into O···H, C···H and H···H intermolecular interactions respectively for the hydrate forms of cyclo-(Sar)$_5$ (**6**) and cyclo-(Sar)$_7$ (**13**).

Hexameric cyclic peptoids

The first hexameric cyclic peptoid to be studied by X-ray crystallography was the cyclo-(Sar)$_6$ (**7**).[26] The sequence of the amide group conformations is *cctcct* (similarly to all other metal-free hexameric cyclic peptoids listed in Table 1 and showed in Fig. 18).

As can been observed in Fig. 19, methyl groups of compound **7** point alternatively up and down with respect to the plane defined by the peptoid backbone.

It is worth noting that the X-ray crystal structure is a methanol solvate. The ratio between cyclopeptoid molecules and methanol molecules is 1:2 (Fig. 20).

Methanol molecules are H-bonded to the oxygen atoms of the *trans* carbonyl groups. The *cis* carbonyl groups oxygen atoms are involved in CH_2···CO interactions among the macrocycles, displaying a typical a *T*-shaped arrangement, with an angle between the planes defined by the peptoid backbone of 80.61°. (Fig. 21).

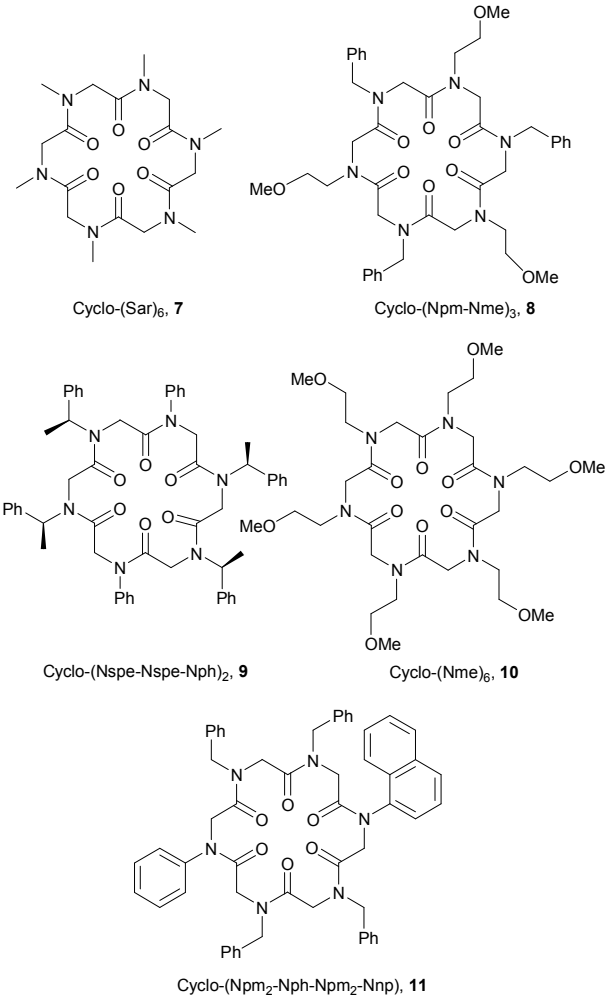

Cyclo-(Sar)$_6$, **7**

Cyclo-(Npm-Nme)$_3$, **8**

Cyclo-(Nspe-Nspe-Nph)$_2$, **9**

Cyclo-(Nme)$_6$, **10**

Cyclo-(Npm$_2$-Nph-Npm$_2$-Nnp), **11**

Fig. 18 Hexameric cyclic peptoids **7**-**11** studied by X-ray crystallography.

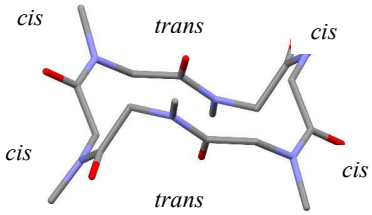

Fig. 19 X-ray molecular structure of cyclo-(Sar)$_6$ (**7**). *Cis* and *trans* amide bonds are indicated.

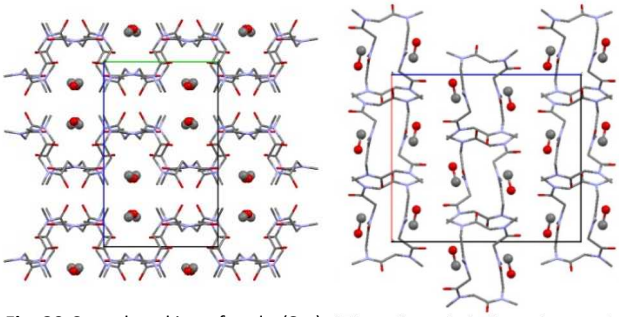

Fig. 20 Crystal packing of cyclo-(Sar)$_6$ (**7**) as viewed a) along the *a* axis and b) along the *b* axis. Hydrogen atoms have been omitted for clarity.

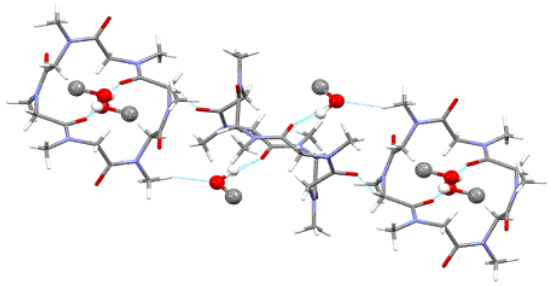

Fig. 21 *T*-shaped arrangement in cyclo-(Sar)$_6$ (7). The angle between the planes defined by the peptoid backbone is 80.61°.

The upper left hydrogen bond spike is determined by CH···O contacts, where the cyclopeptoid molecule acts as a hydrogen bond donor towards methanol molecules (at 2.30 Å distance) or cyclopeptoid molecules (at 2.34 Å). The lower right hydrogen bond spike is determined by OH···O contacts, where the cyclopeptoid molecule acts instead as H-bond acceptor towards methanol molecules (at 1.83 Å distance) or cyclopeptoid molecules (at d_i+ d_e= 2.34 Å, where the green-blue streak appears). Close H···H contacts at 2.18 Å correspond to methyl-methyl contacts.

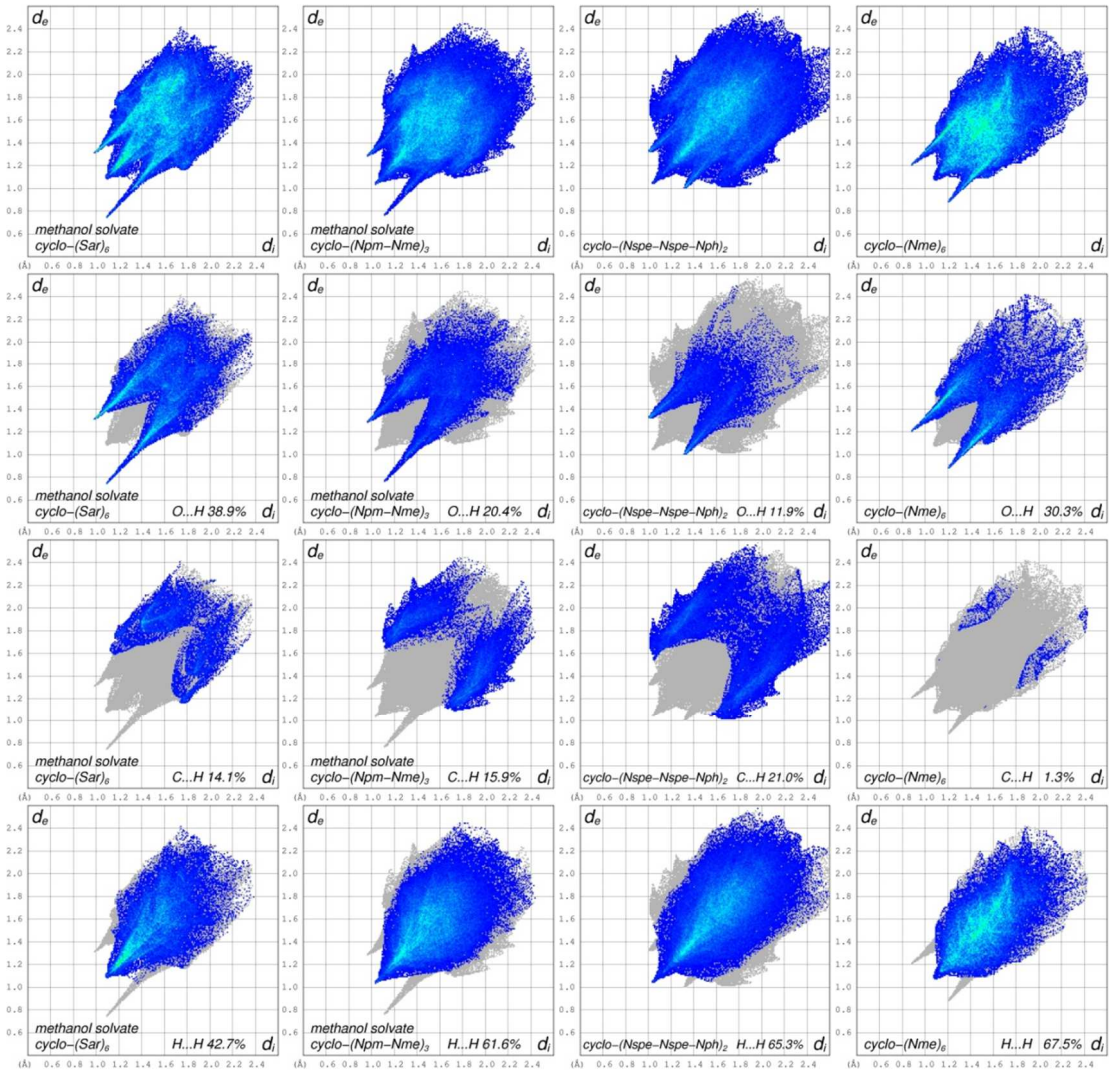

Fig. 22 Comparison of full fingerprint plots and decomposed fingerprint plots into O···H, C···H and H···H intermolecular interactions respectively for cyclo-(Sar)$_6$ (**7**) methanol solvate, cyclo-(Npm-Nme)$_3$ (**8**) methanol solvate, cyclo-(Nspe-Nspe-Nph)$_2$ (**9**), cyclo-(Nme)$_6$ (**10**).

The second hexameric cyclic peptoid to be studied by X-ray crystallography was the cyclo-(Npm-Nme)$_3$ (**8**).[5b] Also in this case the X-ray crystal structure includes methanol molecules (Fig. 23). Similarly to cyclo-(Sar)$_6$ (**7**),[26] the side groups point in opposite directions respect to the plane defined by the peptoid backbone. Polar (methoxyethyl) and nonpolar (benzyl) side chains are clustered on opposite sides of the macrocycle, as shown by Fig 23. Methanol molecules are at the interface between the two sides, being H-bond distance to the oxygen atom of one of the *cis* carbonyl groups (CO···HO 1.87 Å, Fig. 24).

Fig. 22 shows the fingerprint plots of cyclo-(Npm-Nme)$_3$ (**8**) as methanol solvate. The upper left and lower right hydrogen bond spikes are rather different for the same reasons already discussed for cyclo-(Sar) (**7**).

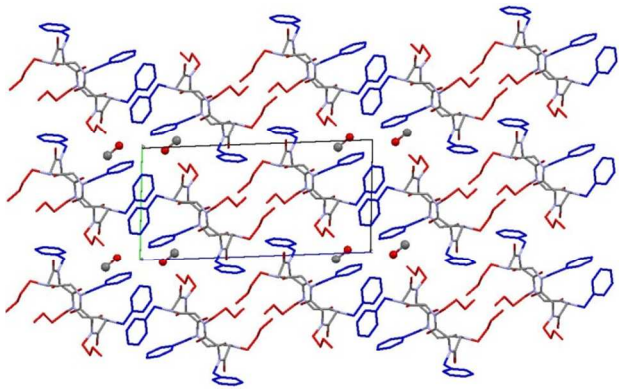

Fig. 23 Crystal packing of cyclo-(Npm-Nme)$_3$ (**8**) as viewed along the *a* axis; polar chains are coloured in red and apolar chains in blue. Hydrogen atoms have been omitted for clarity.

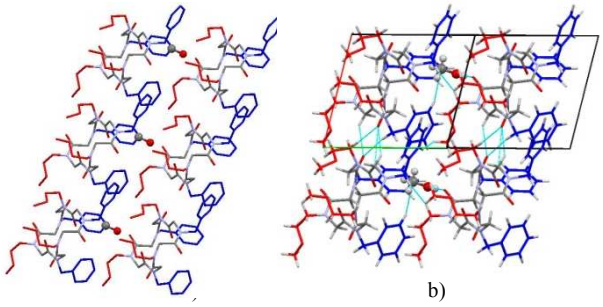

Fig. 24 Cyclo-(Npm-Nme)$_3$ (**8**): a) Interface between polar and nonpolar groups with methanol molecules in between. Hydrogen atoms have been omitted for clarity. b) Intermolecular contacts among macrocycles at the polar/nonpolar interfaces, as viewed along the [011] direction.

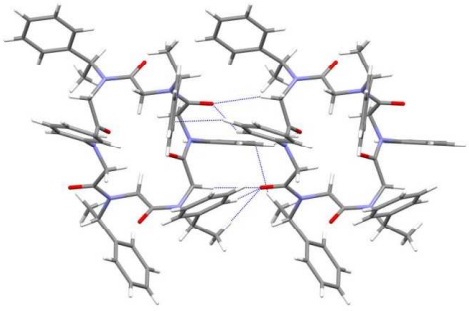

Fig. 25 Cyclo-(Nspe-Nspe-Nph)$_2$ (**9**), CH_2···OC and CH_{ar}···CO side by side contacts along the shortest axis (*a* axis).

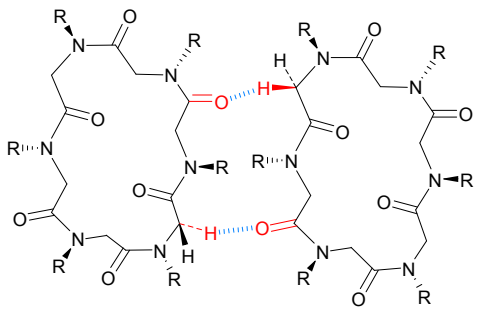

Fig. 26 Side by side arrangement of peptoid macrocycles is provided by CH_2···OC interactions.

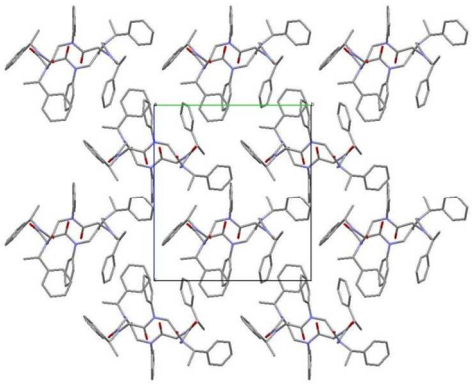

Fig. 27 Crystal packing of cyclo-(Nspe-Nspe-Nph)$_2$ (**9**) as viewed along the *a* axis. Hydrogen atoms have been omitted for clarity.

It is worth noting the different contribution of O···H contacts to the total interactions in the crystal (20.4% for **8** vs. 38.9% for **7**), which is compensated by the corresponding increase of H···H interactions (61.6% for **8** vs. 42.7% for **7**).

The wings characteristic of CH-pi interactions possess a symmetric sawtooth shape, corresponding to different CH-pi interactions involving the three aromatic side groups.

Very close head-to-head H···H contacts at 2.10 Å correspond to contacts among methylene hydrogen atoms and aromatic hydrogen atoms.

In the case of cyclo-(Nspe-Nspe-Nph)$_2$,[27] (**9**) the aryl moieties of two *N*-phenyl residues are perpendicular to the plane defined by the peptoid backbone (Fig. 25).

The presence of aryl groups favours side by side contacts instead of top-bottom contacts (Fig. 25 and 26). Molecules align side by side along the shortest cell axis (*a* axis) by means of hydrogen bond and CH-pi interactions.

Hydrogen bond are established between the oxygen atoms of *cis* carbonyl groups and i) methyl hydrogen atoms at 2.32 Å, ii) aromatic hydrogen atoms at 2.34, iii) methylene hydrogen atoms at 2.51 Å. CH_{ar}-pi interactions are among *N*-phenyl ring hydrogen atoms and aromatic carbon atoms of one *N*-phenyl-ethyl residue and CH_3-pi interactions are among methyl hydrogen atoms of one *N*-phenyl-ethyl residue and the pi system of a *N*-phenyl residue.

CH_{ar}-pi interactions among *N*-phenyl ring hydrogen atoms and aromatic carbon atoms of one *N*-phenyl-ethyl residue extend the packing in the plane perpendicular to the *a* axis (Fig. 27).

Fig. 22 shows the fingerprint plots of cyclo-(Nspe-Nspe-Nph)$_2$ (**9**). The upper left and lower right hydrogen bond spikes are rather short and wide. The contribution of O···H interactions to the total interactions in the crystal is only 11.9%, while C···H interactions amount to 21.9%. Indeed, the wings characteristic of CH-pi interactions appear with a symmetric sawtooth shape, corresponding to CH-pi interactions involving the aromatic side groups. Very close head-to head H···H contacts at 2.07 Å correspond to contacts among methylene hydrogen and aromatic hydrogen atoms.

It is noteworthy the densely coloured blue region between 2.2 Å and 2.4 Å, which accounts for the presence of a large number of long contacts. The plot extends slightly beyond 2.5 Å, indicating a non-optimally dense packing.

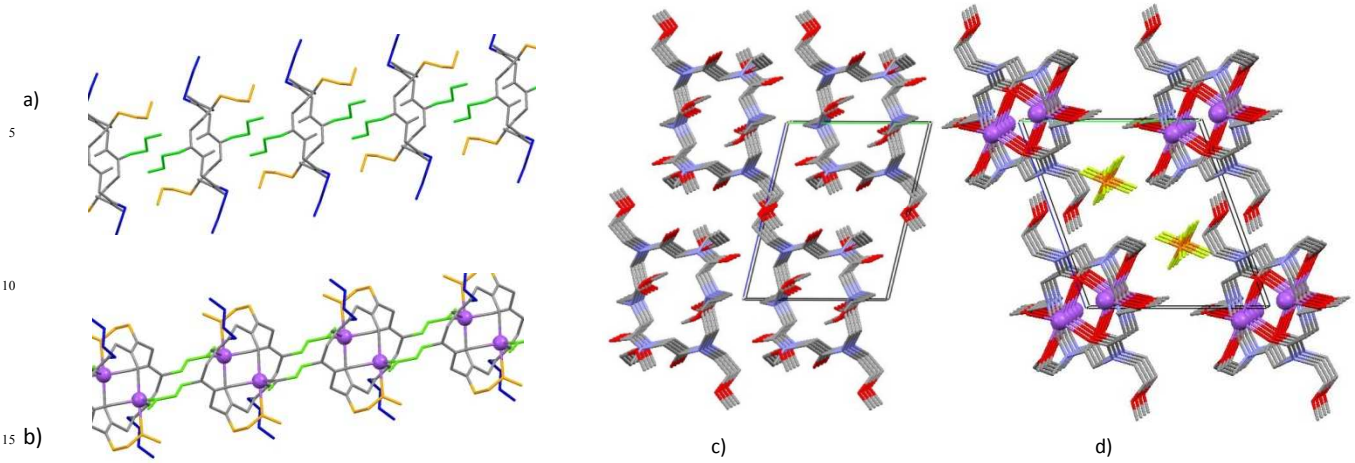

Fig. 28 a) Columnar arrangement of molecules in the cyclo-$(Nme)_6$ (**10**) free form and b) as sodium complex (**10**·Na^+) to form a *1D* coordination polymer. Coloured side-chains highlight the macrocycle pre-organization; c) crystal packing of cyclo-$(NMe)_6$ and d) of the corresponding Na^+ complex as viewed along the *a* axis. PF_6^- anions occupy interstitial spaces. Sodium ions in magenta, phosphorus in orange and fluorine in green. Hydrogen atoms have been omitted for clarity.

In the case of cyclo-$(Nme)_6$ (**10**)[15] we observe two different orientations of the side chains (Fig. 28a). In particular, two side chains extend horizontally and four side chains extend vertically with respect to the plane defined by the peptoid backbone atoms.

Side-by-side arrangement of peptoid tubes is provided by CH_2···OC interactions among peptoid backbone atoms (at 2.08 Å) so that peptoid rings are paired on the same level (Fig. 26).

vertical chains also contribute to the tubular arrangement of the macrocycles along the shortest axis (*a* axis), they interact by means of CH_2···OC interactions between backbone carbonyl groups and side chains methylene hydrogen atoms of the top and bottom macrocycles at a distance of 2.36 Å.

Also horizontal chains contribute to intertubular interactions by means of CH···O interactions with other side chains and CH_2···OC interactions involving backbone carbonyl groups.

Fig. 22 shows the fingerprint plots of cyclo-$(Nme)_6$ (**10**). They are characterized by i) two symmetrical sharp features for CH···OC contacts, which are at 2.08 Å, the closest observed among non-hydrated or non-solvated cyclopeptoids; ii) a central green-blue wide spike for H···H contacts, the closest one being at 2.15 Å, corresponding to contacts among methylene hydrogen atoms of adjacent tubes; iii) a blurred blue region between 2.2 and 2.4 Å.

It is worth noting the significant contribution of O···H contacts to the total interactions in the crystal (30.3% for compound **10**).

Finally, for cyclo-(Npm_2-Nph-Npm_2-Nnp),[28] (**11**) the disorder of the naphthyl group, which can occupy alternatively two opposite positions in the macrocycle, hampers any proper consideration about crystal packing features.

Metal coordination

One of the most interesting features of hexameric cyclic peptoids is their ability to form highly stable metal complexes ($K_a \sim 10^6$ for Na^+, Li^+ and K^+ and $K_a \sim 10^{16}$ for Gd^{+3}).[10,13] The thermodynamically favoured metal-ligand interaction consistently alters the peptoid backbone conformation and dictates highly symmetric conformations. All the X-ray crystal structures of metal complexes show a unique S_6-symmetric *all-trans* peptoid backbone conformation with the carbonyl groups alternately pointing toward the center of the ring to bind the metal cations and with ω dihedral angles slightly deviating from 180°.

On the basis of these considerations, it is appropriate to affirm that metal coordination is one of the most effective way to control the conformation of peptoid macrocycles and an effective way to trigger crystallization.

An exemplar case of metal chelation is that of the cyclo-$(Nme)_6$ Na^+ complex (**10**·Na^+, Fig. 28b).[15] In this metallated adduct the carbonyl groups point towards pentacoordinated sodium ions, two side chains point towards the center of the ring to bind the Na^+ and two further side chains bind contiguous sodium ions giving rise to a *1D* coordination polymer. The remaining other two side chains point outside and are involved in crystal packing interactions

It is worthwhile to note that the tubular arrangement of the free form is preserved in the metallated form in spite of different peptoid backbone conformation.

As can be seen in Fig. 28 a) and b), blue and green side chains do not change direction both in the free and metallated form, while the yellow ones fold towards the centre of the ring to bind sodium ions in the chelated form. Ring centroid-centroid distances along the tubes are very similar: 8.358 Å in the free form and 8.805 Å in the Na^+ complex.

PF_6^- anions are located among the nanotubes (Fig. 28 d), they are involved in weak hydrogen bonds with side chains methylene and methyl groups.[18c,29]

Therefore, intertubular distances in one direction increase from 9.176 Å, in the free form, to 12.477 Å, in the Na^+ complex, while in the other direction they are very similar in both the cases (11.623 Å against 11.014 Å).

The role of the counterion can be appreciated considering the X-ray crystal structure of cyclo-$(Nbe)_6$ (**12**, Fig. 29) complexed with the Sr^{2+} ion (**12**·Sr^{2+}).[13]

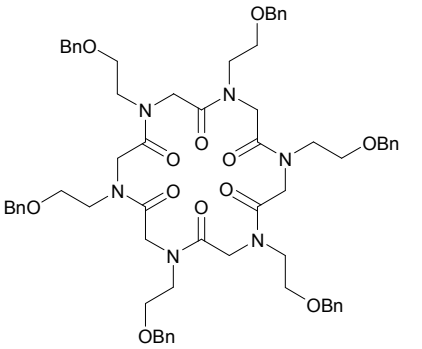

Cyclo-(Nbe)$_6$, **12**

Fig. 29 Hexameric cyclic peptoid **12** forming a complex with Sr^{2+}.

In this zwitterionic complex three Sr^{2+} cations are sandwiched among two cyclopeptoid molecules, six picrate anions behave as a bidentate ligand completing the coordination sphere of the Sr^{2+} cations (Fig. 30a).

Also in this case the peptoid backbone conformation is all-*trans* and the carbonyl groups alternately point toward the Sr^{2+} cations and force the *N*-linked side chains to assume an alternate pseudo-equatorial arrangement, which allows the stacking of the macrocycles with a ring centroid-centroid distance of 4.756 Å.

The stacking is interrupted by the picrate anions, which are bonded to the edge strontium cations.

Two water molecules, H-bonded to side chain oxygen atoms, are entrapped among the benzyloxy spires.

The zwitterionic complex exposes outwards the picrate and benzyl moieties, which are responsible of the packing interactions by means of hydrogen bonds and CH-pi interactions. (Fig 30b).

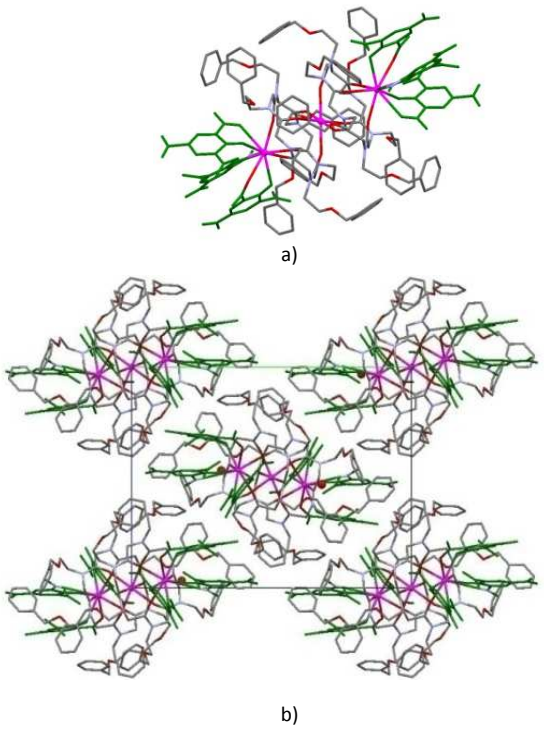

a)

b)

Fig. 30 a) Cyclo-(Nbe)$_6$ Sr^{2+} picrate zwitterionic complex; Sr^{2+} cations are in magenta and picrate anions are in green; b) crystal packing as viewed along the *a* axis. Hydrogen atoms have been omitted for clarity.

Heptameric cyclic peptoids

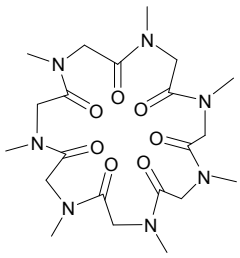

Cyclo-(Sar)$_7$, **13**

Fig. 31 Heptameric cyclic peptoid cyclo-(Sar)$_7$ **13** studied by X-ray crystallography.

The only known X-ray crystal structure of heptameric cyclic peptoid is that of cycloeptasarcosyl monohydrate, cyclo-(Sar)$_7$ (**13**, Fig. 31).[30]

As reported in Table 1, the ring conformation is *ccccttt*, this represents the only example of metal free cyclic peptoid with three consecutive *trans* amide bonds.

The crystal packing is characterized by the tubular arrangement of cyclopeptoid and water molecules along the *c* axis (Fig. 32 and 33). This is determined mainly by hydrogen bonds involving two *trans* carbonyl groups and two water molecules, which are located respectively above and below the plane formed by the peptoid backbone. Side by side intertubular contacts are provided by *cis* carbonyl groups, which interact with methylene hydrogen atoms of a sideward cyclopeptoid molecule.

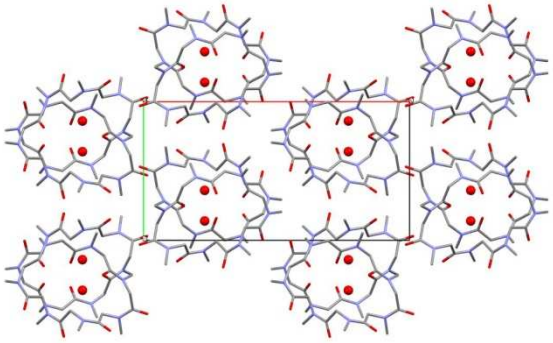

Fig. 32 Crystal packing of cyclo-(Sar)$_7$ (**13**) as viewed along the *c* axis. Hydrogen atoms have been omitted for clarity.

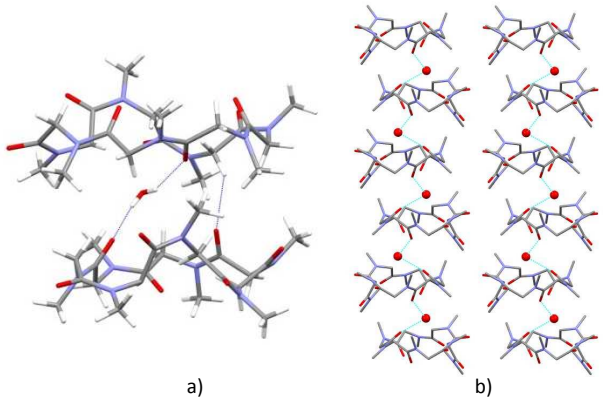

a) b)

Fig. 33 a) Hydrogen bonds involving water molecules and $CH_2\cdots CO$ interactions are responsible of the self assembly of cyclo-(Sar)$_7$ (**13**) and water molecules into a tubular architecture; b) tubular arrangement along the *c* axis.

Fig. 17 shows also the fingerprint plots of the hydrate form of cyclo-(Sar)$_7$ (**13**), it refers only to the cyclopeptoid molecules and for this reason it is rather unsymmetrical.

The upper left hydrogen bond spike is barely visible, it corresponds to CH···O contacts, which are at a rather longer distance than OH···O contacts (2.38 Å vs. 1.89 Å). Notably CH···O contacts show values more similar to the anhydrous form of cyclo-(Sar)$_4$ (**3**) (Fig. 8) then to the hydrate form of cyclo-(Sar)$_5$ (**6**) (Fig. 17).

Close H···H contacts are between methyl hydrogen atoms at 2.18 Å. The plot extends beyond 2.4 Å with a blurred blue tail, indicating a non-optimally dense packing.

Octameric cyclic peptoids

As reported in Table 1, the X-ray crystal structures of the three octameric cyclic peptoids cyclo-(Sar)$_8$ (**14**),[31] cyclo-(Npm-Nme)$_4$ (**15**)[5b] and cyclo-(Npa-Nme-Nph-Nph)$_2$ (**16**)[14] (Fig. 34), show four *cis* and four *trans* amide bonds in the peptoid backbone.

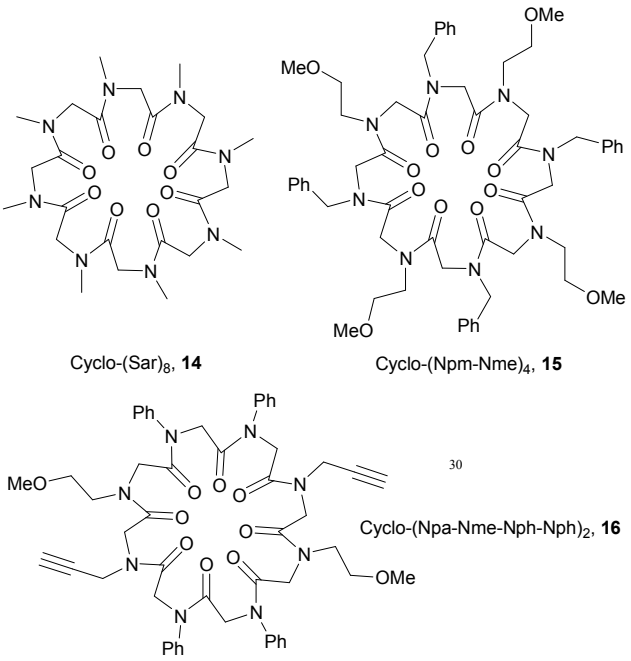

Fig. 34 Octameric cyclic peptoids **14-16** studied by X-ray crystallography.

As reported in Table 1, the X-ray crystal structures of the three octameric cyclic peptoids cyclo-(Sar)$_8$ (**14**),[31] cyclo-(Npm-Nme)$_4$ (**15**)[5b] and cyclo-(Npa-Nme-Nph-Nph)$_2$ (**16**)[14] (Fig. 34), show four *cis* and four *trans* amide bonds in the peptoid backbone.

The first two compounds display an approximate C_2 molecular symmetry, for the third one the C_2 symmetry is imposed by crystal symmetry.

The overall morphology of the cyclo-octapeptoid backbone is similar to that of a "butterfly".

The first X-ray crystal structure to be studied was that of cyclo-(Sar)$_8$ (**14**) and it corresponded to a tetrahydrate form.[31]

A supramolecular dimer of cyclopeptoid molecules is formed by means of intermolecular CH_2···OC hydrogen bonds.

Water molecules are clustered in teteramers, each dimer is connected by means of hydrogen bonds to six water tetramers in a rather approximate octahedral fashion. (Fig. 35)

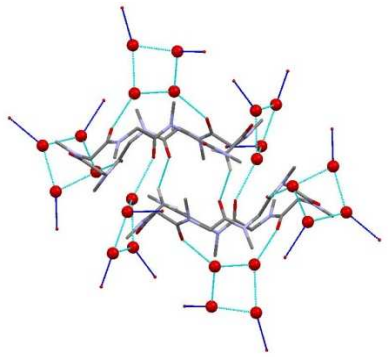

Fig. 35 Cyclo-(Sar)$_8$ (**14**) dimer are surrounded by water clusters by means of hydrogen bonds (light blue). Blue lines indicate hydrogen bond connections to other cyclopeptoid dimers. Hydrogen atoms have been omitted for clarity.

The crystal packing can be described considering that cyclopeptoid dimers alternate with water tetramers along the three axes to form a three dimensional hydrogen-bonded interconnected network (Fig. 36).

For the hydrate form of cyclo-(Sar)$_8$ (**14**) methyl hydrogen atoms could not be located, trying to add them in calculated position unfortunately did not allow to provide a meaningful Hirshfeld fingerprint plot (too short H···H contacts resulted).

In the crystal structure of cyclo-(Npm-Nme)$_4$ (**15**)[5b] there are two crystallographically independent molecules, which differ by side chains conformations (in particular those of the benzyl groups).

In both molecules two methoxyethyl and two benzyl side chains extend vertically with respect to the plane defined by peptoid backbone atoms (Fig. 37).

Vertical benzyl side chains are mutually included inside the cavity created by methoxyethyl groups by means of CH_{ar}···OC hydrogen bonds and CH_3-pi interactions (see Fig. 38, shortest contacts are: CH_{ar}···OC 2.32 Å, 2.54 Å, 2.57 Å and CH_3···C_{ar}: 2.65 Å, 2.70 Å).

These interactions give rise to a tubular arrangement of cyclopeptoid molecules along the *b* axis.

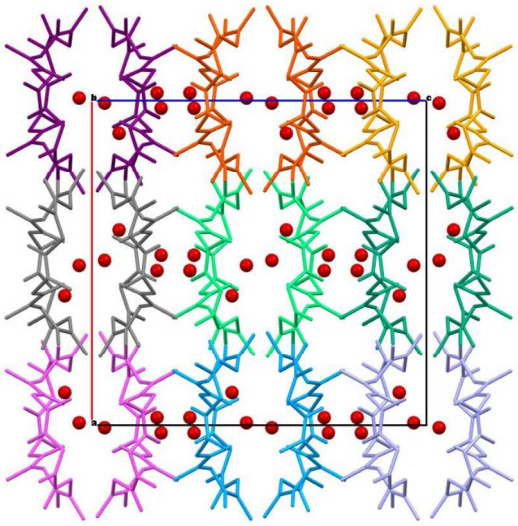

Fig. 36 Crystal packing of cyclo-(Sar)$_8$ (**14**) tetrahydrate as viewed along the *b* axis. Molecules forming dimers have the same colour. Hydrogen atoms have been omitted for clarity.

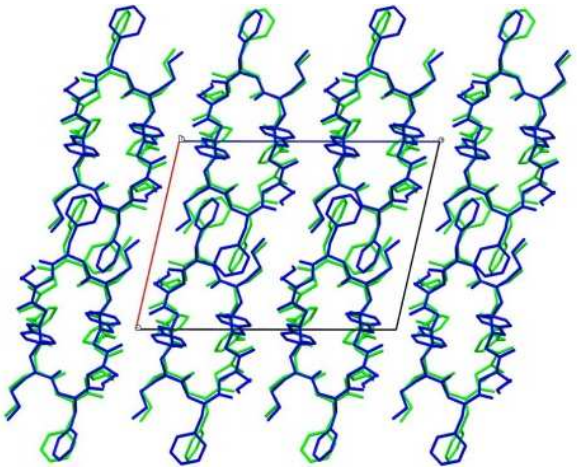

Fig. 37 Crystal packing of cyclo-(Npm-Nme)$_4$ (**15**) as viewed along the *b* axis. Hydrogen atoms have been omitted for clarity.

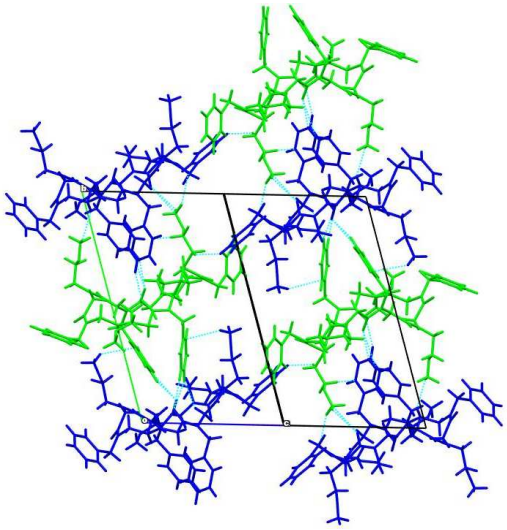

Fig. 38 Crystal packing of cyclo-(Npm-Nme)$_4$ (**15**) a) as viewed along the [101] direction, side chains interactions are coloured in light blue.

As there are two independent molecules in the asymmetric unit (Z'=2) two Hirshfeld fingerprint plots are provided for each independent molecule in Fig 39. It is evident that a much narrower plot is obtained in the case of molecule I with d_i and d_e values ranging from 1.1 Å to 2.6 Å, while in the case of molecule II d_i and d_e values extend till 2.8 Å, indicating that molecule I is involved in closer contacts than molecule II. As already observed for cyclo-(Sar)$_3$ (**1**) and cyclo-(Nal)$_3$ (**3**), the two fingerprint plots of cyclo-(Npm-Nme)$_4$ (**15**) in Fig. 39 result to be unsymmetrical. A closer inspection reveals that, for both compounds **1** and **2,** the features at the upper left of the fingerprint plot for molecule I are identically reproduced in the lower right of the fingerprint plot for molecule II and vice versa.

In details, the upper left hydrogen bond spike for molecule I is identical to the lower right hydrogen bond spike for molecule II: this means that molecule I acts as a hydrogen bond donor towards molecule II. Correspondingly the upper left hydrogen bond (broad) spike for molecule II is identical to the lower right hydrogen bond spike for molecule I: this means that molecule II acts as a hydrogen bond donor towards molecule I.

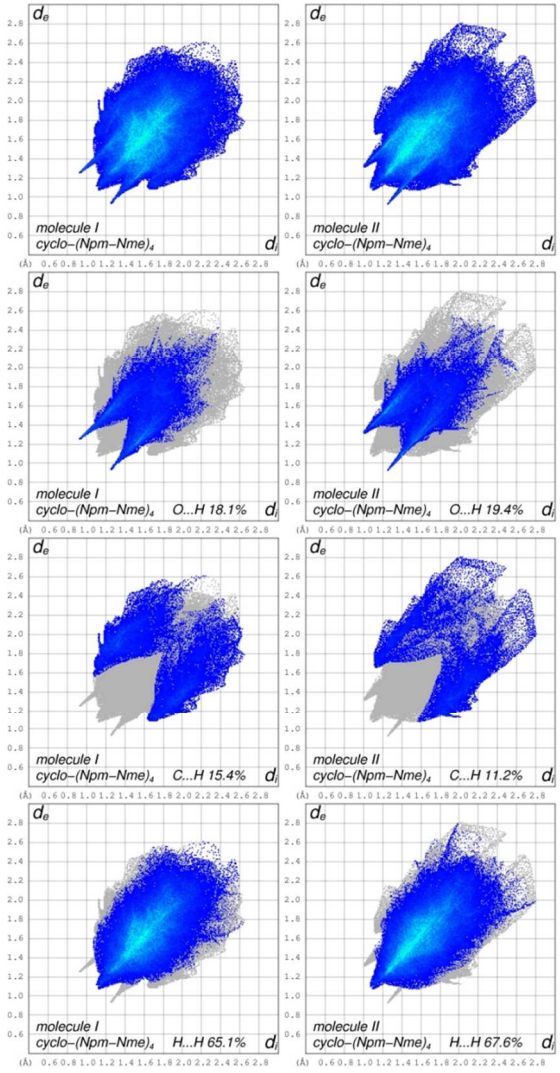

Fig. 39. Comparison of full fingerprint plots and decomposed fingerprint plots into various intermolecular interactions of cyclo-(Sar)$_8$ hydrate (**14**) and cyclo-(Npm-Nme)$_4$ (**15**).

The same holds for C···H contacts, the sharp feature, which appears in the left wing of the fingerprint plot of molecule I, can be found in the right wing of molecule II. It corresponds to the CH-pi interaction, which is involved in the tubular arrangement of the cyclopeptoid molecules and depicted in Fig. 38, where molecule I is the blue one and molecule II is the green one.

The closest H···H contacts are at 2.16 Å involving methylene hydrogen atoms and aromatic hydrogen atoms.

In the case of cyclo-(Npa-Nme-Nph-Nph)$_2$ (**16**),[14] the *N*-phenyl side chains provide a *trans* amide conformation, while the *N*-alkyl peptoid residues gives *cis* amide linkages. The *N*-propargyl side chains and two *N*-phenyl side chains extend vertically above and below the macrocycle plane (Fig. 40).

Thus cyclopeptoids arrange in a tubular architecture, forming hollow cylinders, where water molecules can be located. Water molecules have not a predominant role in the crystal packing of the hydrate form, indeed they can be completely removed without disrupting the crystal architecture.

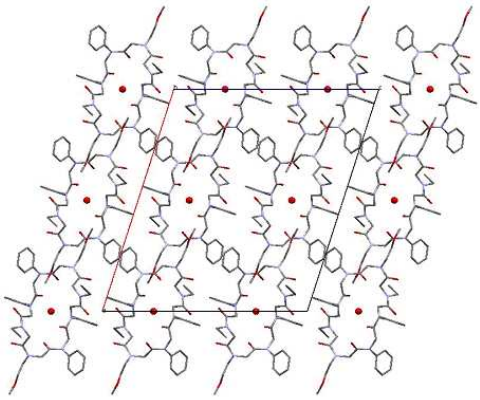

Fig. 40 Crystal packing of cyclo-(Npa-Nme-Nph-Nph)$_2$ (**16**) as viewed along the *b* axis. Hydrogen atoms have been omitted for clarity.

Two *N*-phenyl side chains are located differently from the usually favoured orientation perpendicular to the amide backbone.[27] They provide intertubular connections by means of CH-pi interactions with backbone methylene hydrogen atoms of side cyclopeptoid molecules. Other side by side connections are provided by methoxyethyl side chains, which bind backbone methylene hydrogen atoms. Thus, peptoid cylinders result to be interdigitated.

The crystal packing of the corresponding dehydrated compound does not show any significant difference from the hydrate form, only void cavities of almost 50 Å^3 volume can be detected in the positions previously occupied by water molecules. This provides an excellent proof that hydrogen bonded water molecules are not essential for building the crystal.

Hirshfeld fingerprint plots in Fig. 41 for cyclo-(Npa-Nme-Nph-Nph)$_2$ (**16**), in its anhydrous and hydrate form, highlight the role of water molecules to the intermolecular interactions in the hydrate form. Most of the differences appear in the decomposed fingerprint plot related to O···H contacts, as for the anhydrous form two symmetrical spikes appear, reaching 2.15 Å. They correspond to O···H$_2$C contacts between the methoxyethyl oxygen atoms and backbone methylene hydrogen atoms at 2.15 Å. As for the hydrate form, two other spikes arise. The longest is related to CO···HO contacts between two carbonyl groups of the cyclopeptoid molecule and one water molecule at 1.89 Å. The shorter and broader spike corresponds to CH$_{ar}$···O contacts, where the water molecules act as acceptor towards aromatic hydrogen atoms at 2.58 Å distance.

Water molecules in the hydrate form take part also in close H···H contacts (at 2.17 Å), that give rise to the slightly unsymmetrical feature of the corresponding decomposed plot. Notably in the anhydrous form H···H no contacts below 2.26 Å are observed.

Additional pi-pi contacts (C···C 3.41 and 3.37 Å) give rise to the green blue central mark, superimposing to the area where H···H also appear.

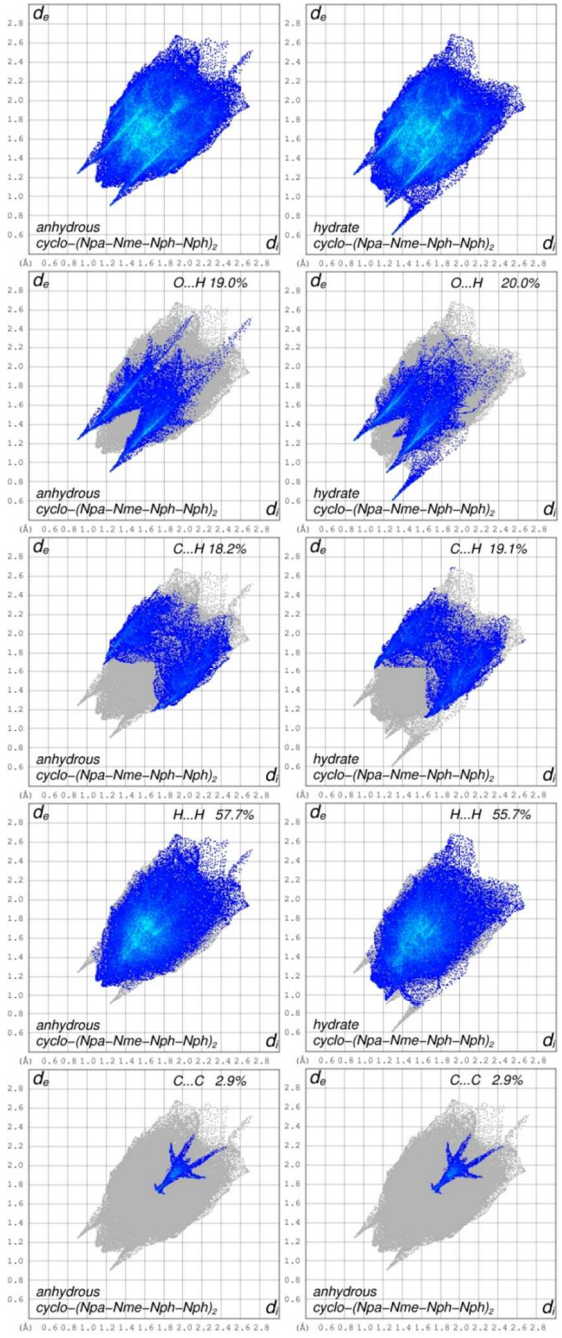

Fig. 41 Comparison of full fingerprint plots and decomposed fingerprint plots into various intermolecular interactions of cyclo-(Npa-Nme-Nph-Nph)$_2$ (**16**) in its anhydrous and hydrate form.

Nonameric cyclic peptoids

There is only one example of X-ray crystal structure for a nonameric cyclic peptoid: this is the cyclo-((*S*)-*N*-(1-phenylethyl)glycine)$_9$ (**17**, Fig. 42), as ethanol solvate (Fig. 43).[32] As reported in Table 1 the ring conformation is *cccctccct*. Four side chains are on one side of the macrocycle plane and five side chains are on the other side (Fig. 43).

The ethanol molecules present in the crystal structure are hydrogen bonded to carbonyl groups and provide also efficient

CH-pi interaction with the side chains aromatic rings. The ratio between cyclopeptoid and ethanol molecules is 1:4.

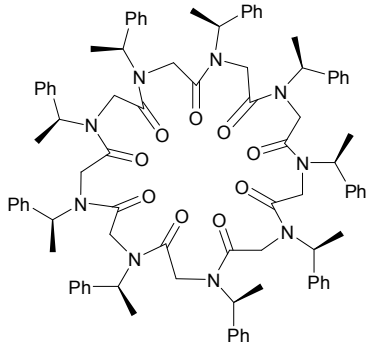

Cyclo-(Nspe)$_9$, **17**

Fig. 42 Nonameric cyclic peptoid **17** studied by X-ray crystallography.

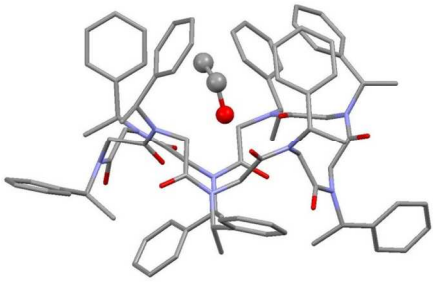

Fig. 43 X-ray molecular structure of cyclo(Nspe)$_9$ (**17**) with an ethanol molecule included in the basket formed by top side chains. Hydrogen atoms have been omitted for clarity.

).

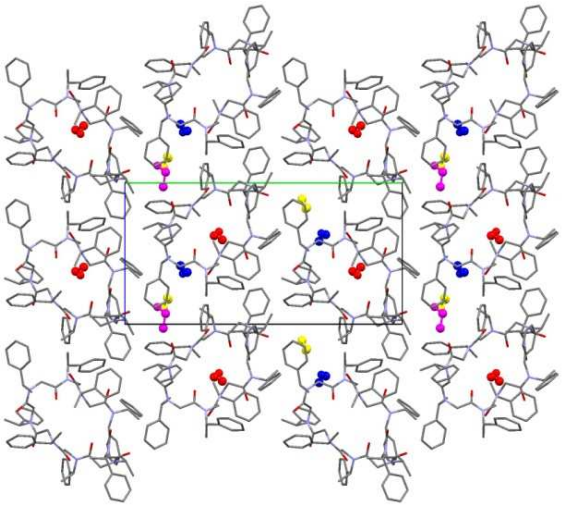

Fig. 44 Crystal packing of cyclo-(Nspe)$_9$ (**17**), as viewed along the *a* axis. Hydrogen atoms have been omitted for clarity.

One ethanol molecule is included among the five side chains, which act as a basket (Fig. 43).

Macrocycles are aligned along the *a* axis by means of CH-pi interactions, forming columns with the basket face on top and columns with the basket face at the bottom, which alternate along the *b* axis. The other three ethanol molecules occupy the cavities among columns (Fig. 44).

Fig. 45 shows the fingerprint plots of cyclo-(Nspe)$_9$ (**17**) ethanol solvate. The upper left and lower right hydrogen bond spikes are rather different, as a consequence of the additional contribution of ethanol molecules to the O···H interactions with the cyclopeptoid molecule acting as H-bond acceptor.

Indeed, the wings characteristic of CH-pi interactions on the left side are also less defined than those on the right side of the fingerprint plot. This is due to the role played by methanol molecules as CH- donor towards the aromatic moieties of the cyclopeptoid molecule.

Very close H···H contacts can be ascribed to the presence of disorder of one aromatic moiety at the bottom of the basket.

The plot extends slightly up to 2.5 Å, indicating a non-optimally dense packing.

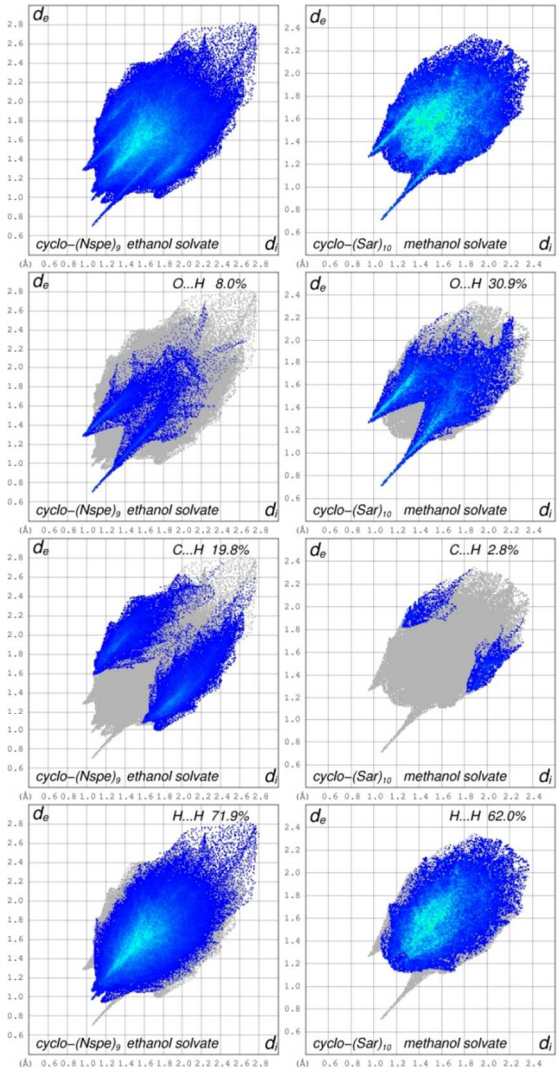

Fig. 45 Comparison of full fingerprint plots and decomposed fingerprint plots into various intermolecular interactions of cyclo-(Nspe)$_9$ ethanol solvate (**17**) and cyclo-(Sar)$_{10}$ (**18**) methanol solvate.

Decameric cyclic peptoids

Only one example of X-ray crystal structure for a decameric cyclic peptoid is reported: this is the cyclo-$(Sar)_{10}$ (**18**, Fig. 46), crystallized as methanol solvate.[33]

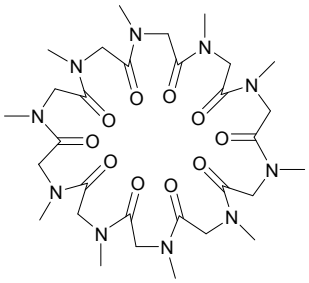

Cyclo-$(Sar)_{10}$, **18**

Fig. 46 Decameric cyclic peptoid **18** studied by X-ray crystallography.

As reported in Table 1 the sequence of amide bonds in the peptoid backbone is: *cccttccctt*, *i.e.* a double repetition of the sequence observed in the pentameric cyclic peptoid (**5**).

The macrocycle possesses a crystallographic inversion centre and exhibits a rather elongated and flattened shape.

The molecules aligns in a tubular arrangement along the *a* axis (with the macrocycle plane inclined by 34° with respect to the *a* axis) through CO···HC interactions between carbonyl groups and both methylene and methyl hydrogen atoms of the cyclopeptoid molecules (respectively at 2.22 Å and 2.41 Å) (Fig. 47a and 48).

Side by side interactions along the *b* axis are provided by methylene hydrogen atoms and carbonyl groups oxygen atoms at 2.29 Å distance (Fig. 47b).

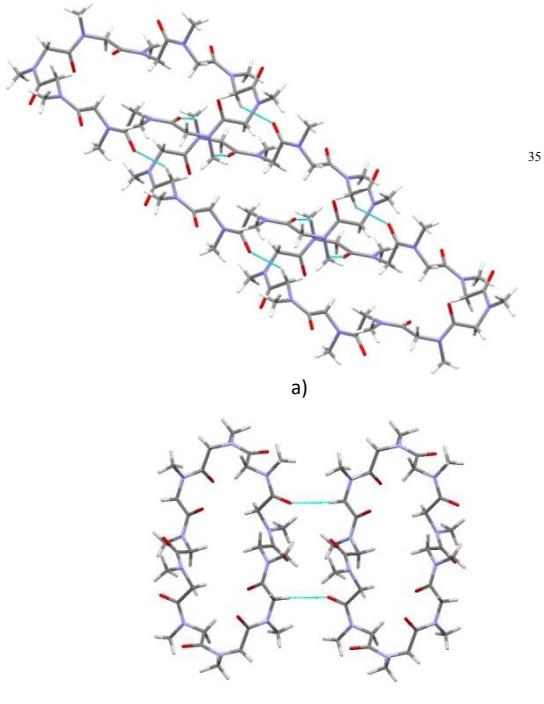

a)

b)

Fig. 47 Details of the interactions along the *a* axis and along the *b* axis for cyclo-$(Sar)_{10}$ (**18**).

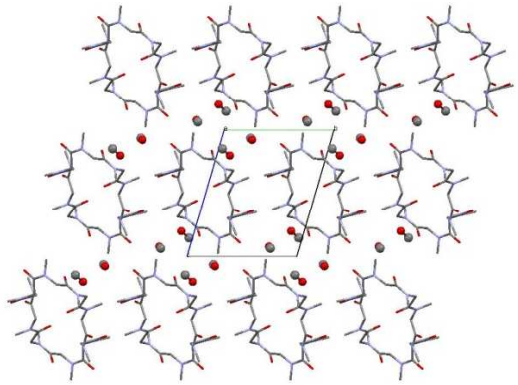

Fig. 48 Crystal packing of cyclo-$(Sar)_{10}$ (**18**) as viewed along the *a* axis. Hydrogen atoms have been omitted for clarity.

The ratio between cyclopeptoid and methanol molecules is 1:2. A channel of methanol molecules is formed along the *a* axis (Fig. 48). One methanol molecule is hydrogen bonded to a *cis* carbonyl oxygen atom and to the other methanol molecule.

Fig. 45 shows the fingerprint plots of cyclo-$(Sar)_{10}$ (**18**) methanol solvate, (it refers only to the cyclopeptoid molecules and for this reason it is rather unsymmetrical).

The upper left hydrogen bond spike is determined only by CH···O contacts, where the cyclopeptoid molecule acts as hydrogen bond donor towards other cyclopeptoid or methanol molecules (with the shortest contact at 2.22 Å).

The lower right hydrogen bond spike is determined by CO···H contacts, where the cyclopeptoid molecule acts as H-bond acceptor instead and both methanol or cyclopeptoid molecules can act as H-bond donors, the former at a shorter distance (1.77 Å), the latter at longer distance (2.22 Å, where the green-blue streak appears and the strike broadens).

Close H···H contacts at 2.33 Å correspond to methyl-methyl contacts.

Conclusions

Cyclic peptoids hold the attention of both synthetic and supramolecular chemists for their elegant and intriguing architectures. This survey allowed us to define many common features of the solid state assembly of cyclic α-peptoids

The peptoid backbone conformation in the solid state seems to not vary that much within macrocycles with the same ring size, with the only notable exception of cyclohexamer metal complexes.

The lack of the amide proton prevents the formation of NH···OC hydrogen bonds and weaker interactions play a key role. Inter-annular CH···OC hydrogen bonds can provide face to face or side by side arrangement of macrocycles in a way that can be considered the peptoid counterpart of β-sheet secondary structure in proteins.

Side chains have a strong influence on the solid state assembly of peptoid macrocycles. Benzyloxyethyl as side chains are able to promote the tubular arrangement of the macrocycles in a face to face arrangement, since they extend horizontally with respect to the macrocycle plane and do not interact with the peptoid

backbone atoms. This results in the formation of a peptoid nanotube by tight stacking of macrocycles.

Side chains may also provide competing interactions to CH···OC inter-annular hydrogen bonds

We observed that, if methyl and benzyl side chains are present, molecular interactions determine often a *T*-shaped arrangement, involving the backbone atoms of a cyclopeptoid molecule and the side chains atoms of another neighbouring cyclopeptoid molecule.

Methoxyethyl and propargyl side chains are able to induce a tubular arrangement of peptoid macrocycles by acting as pillars, they can extend vertically with respect to the macrocycle plane and interact with the backbone atoms belonging to the above or below macrocycles.

Thus, the choice of side chains appears to be crucial to define the solid state assembly of α-cyclic peptoids.

Also the size of the macrocycle contributes to promote a tubular arrangement: as the size of the macrocycle increases, side by side arrangement of macrocycles is favoured over a *T*-shaped arrangement.

The occurrence of hydrate or solvate forms among cyclic peptoids is rather common. Solvent molecules are key components of the crystal architecture of cyclic peptoids, less usually they can be removed without destroying the crystal, as it happens for the highly thermostable cycloctamer.

Although no case of polymorphism has been reported up to now for cyclic peptoids, it is likely that this will change in the next future as research in the field progresses.

Hirshfeld fingerprint analysis allowed to study the interplay of weak intermolecular interactions, as weak CH···OC hydrogen bonds and CH-pi interactions, and their quantitative contributions towards the crystal packing.

Experimental

General information

Reactions involving air or moisture sensitive reagents were carried out under nitrogen atmosphere using freshly distilled solvents. Toluene and dichloromethane were distilled from calcium hydride under nitrogen. Glassware was flame-dried (0.05 Torr) prior to use. When necessary, compounds were dried in vacuo over P_2O_5, by azeotropic removal of water with toluene under reduced pressure. Starting materials and reagents purchased from commercial suppliers were generally used without purification. HPLC analysis were performed on a C_{18} reversed-phase analytical and semipreparative columns (Waters, Bondapak, 10 μm, 125 Å 3.9 mm × 300 mm and 7.8 × 300 mm, respectively) using a Modular HPLC System JASCO LC-NET II/ADC equipped with a JASCO Model PU-2089 Plus Pump and a JASCO MD-2010 Plus UV–vis multiple wavelength detector set at 220 nm.

Yield refer to chromatographically and spectroscopically (^{1}H and ^{13}C NMR) pure materials. The NMR spectra were recorded on DRX 250 (^{1}H at 250.13 MHz, ^{13}C at 62.89 MHz) spectrometers. Chemical shifts (δ) are reported in ppm relatively to the residual solvent peak ($CHCl_3$, δ = 7.26, $^{13}CDCl_3$, δ = 77.0 and the multiplicity of each signal is designated by the following abbreviations: s, singlet; d, doublet; t, triplet; q, quartet; quint, quintuplet; m, multiplet; br, broad signal. Coupling constants (*J*) are quoted in hertz. High resolution ESI-MS spectra were performed on a Q-Star Applied Biosystem mass spectrometer. ESI-MS analysis in positive ion mode was performed using a Finnigan LCQ Deca ion trap mass spectrometer (ThermoFinnigan, San Josè, CA, USA) and the mass spectra were acquired and processed using the Xcalibur software provided by Thermo Finnigan.

Solid-phase synthesis of the linear precursor of cyclotetra-*N*-benzylglycine

Linear peptoid tetramer was synthesized using a sub-monomer solid-phase approach. The 2-chlorotrityl chloride resin (2,α-dichlorobenzhydryl-polystyrene crosslinked with 1% DVB; 100–200 mesh; 1.2 mmol/g, 0.20 g, 0.24 mmol) was swelled in dry CH_2Cl_2 (2 mL) for 45 min and washed twice with dry DMF (2 mL). The first sub-monomer was attached onto the resin by adding bromoacetic acid (40 mg, 0.29 mmol) in dry CH_2Cl_2 (2 mL) and of DIPEA (167 μL, 0.96 mmol) on a shaker platform for 40 min at room temperature, followed by washing with dry CH_2Cl_2 (2 mL) and then with DMF (3 × 2 mL). To the bromoacetylated resin was added a DMF solution of the benzylamine amine (10 eq, 257 mg, 2.40 mmol), 1 M in DMF. The mixture was left on a shaker platform for 40 min at room temperature, then the resin was washed with DMF (3 × 2 mL). Subsequent bromoacetylation reactions were accomplished by reacting the aminated oligomer with a solution of bromoacetic acid (10 eq, 333 mg, 2.40 mmol) in DMF (2 mL) and of DIC (11 eq, 0.410 mL, 2.64 mmol) for 40 min at room temperature. The filtered resin was washed with DMF (3 × 2 mL) and treated again with the amine under the same conditions reported above. This cycle of reactions was iterated until the tetramer was obtained. The cleavage was performed by treating twice the resin, previously washed with CH_2Cl_2 (3 × 2 mL), with a solution of HFIP in CH_2Cl_2 (20% v/v, 8 mL) on a shaker platform at room temperature for 40 min and 5 min, respectively. The resin was then filtered away and the combined filtrates were concentrated in vacuo, giving an amorphous white solid. The final product was dissolved in 50% acetonitrile in HPLC grade water and analyzed by RP-HPLC [purity >95%; conditions: 5→100% B in 30 min for oligomers flow: 1 mL/min, 220 nm minutes (A: 0.1% TFA in water, B: 0.1% TFA in acetonitrile)]; t_R: 15.4 min. The linear oligomer was subjected to the cyclization reaction without further purification. Crude linear precursor: 84.0 mg (58% yield); ES-MS: 607.0 *m/z* $[M + H]^+$.

Cyclization reaction: synthesis of cyclo-(Npm)$_4$, 5

To a solution of the linear precursor (37 mg, 0.061 mmol) in dry DMF (3 mL) at room temperature, a mixture of PyBOP (127 mg, 0.244 mmol) and DIPEA (66 μL, 0.379 mmol) in dry DMF (17 mL) was added drop-wise by syringe pump in 1 h. After 12 h the resulting mixture was concentrated in vacuo, diluted with CH_2Cl_2 (16.0 mL) and a solution of HCl (0.5 M, 8.0 mL). The mixture was extracted with CH_2Cl_2 (2 × 16.0 mL) and the combined organic phases were washed with water (40.0 mL), dried over anhydrous $MgSO_4$, filtered and concentrated in vacuo. The cyclic product was dissolved in 50% acetonitrile in HPLC grade water and analyzed by RP-HPLC [purity >95%; conditions: 5→100% B in 30 min for oligomers flow: 1 mL/min, 220 nm minutes (A:

0.1% TFA in water, B: 0.1% TFA in acetonitrile)]; t_R: 18.0 min. The crude residue was purified by precipitation in acetonitrile/water: 1/1.

5: 15.8 mg (44% yield); white amorphous solid; HR-ESI MS: *m/z* 589.2877 $[M+H]^+$(calcd for $C_{36}H_{37}N_4O_4^+$ 589.2809); ES-MS: 589.4 *m/z* $[M+H^+]$; 611.7 *m/z* $[M+Na^+]$; ^{1}H-NMR: (250 MHz, $CDCl_3$) δ: 7.23 (20 H, m, *H*-Ar), 5.55 (2 H, br d, *J* =14.0 Hz, -NC*H*HCO), 5.40 (2 H, br d, *J* = 14.5 Hz, -NC*H*HCO), 4.40 (6 H, m, -CH_2Ph), 3.72 (2 H, br d, *J* = 14.0 Hz, -NCH*H*CO), 3.50 (4 H, m, -NCH*H*CO, -CH_2Ph). ^{13}C-NMR: (66 MHz, $CDCl_3$) δ: 169.1(*C*O × 2), 168.0 (*C*O × 2), 135.9 (C_q-Ar × 2), 135.3 (C_q-Ar × 2), 129.1 (*C*-Ar × 8), 128.8 (*C*-Ar × 4), 128.0 (*C*-Ar × 2), 127.9 (*C*-Ar × 2), 126.7 (*C*-Ar × 4), 50.5 (× 2), 49.3 (× 2), 49.0 (× 2), 47.3 (× 2).

X-ray crystallography

White pyramidal crystals (0.3 x 0.3 x 0.4 mm) of cyclo-$(Npm)_4$ (**5**) were obtained by slow evaporation of a dichloromethane solution. Diffraction data were collected with a Rigaku AFC11K diffractometer equipped with a Saturn944 CCD detector using Cu *K*α radiation. 8920 reflections were measured, of which 2253 are independent reflections (R_{int} 0.045).

Data reduction was performed with the crystallographic package CrystalClear.[34]

The structure was solved by direct methods using the program SIR2002[35] and refined by means of full matrix least-squares based on F^2 using the program SHELXL97.[36]

All non-hydrogen atoms were refined anisotropically, hydrogen atoms were positioned geometrically and included in structure factors calculations but not refined. A total of 200 refinable parameters were finally considered. Maximum and minimum residual density were respectively - 0.26 and 0.23 e/Å^3.

Final disagreement indices: $R1 = 0.059$ for 1985 reflections with $I > 2\sigma_I$, $_wR2 = 0.22$ for 2253 reflections.

X-ray crystal structures for cyclo-$(Npm)_4$ (**5**) and all other compounds discussed in this work are drawn by means of the program Mercury.[37]

Hirshfeld surface analysis

All crystal structures are obtained from CSD November 2013 release, with exception of the new compound **5** and compound **9** (whose cif file was retrieved from the publisher).

Hirshfeld surface analysis and related fingerprint plots have been performed with Crystal Explorer 3.1.[38] To compare related structures the lengths of X-H bonds are normalized using standard X–H distances from Allen *et al*.[39] Thus, X-H distances and X...H contacts are not equal to those calculated from original cif files. Reported X-H distances and X...H contacts refer always to those calculated by Crystal Explorer 3.1 to allow a direct reference with the corresponding Hirshfeld fingerprint plots.

Acknowledgements

We wish to acknowledge Mr. M. Amendola and Mr. G. Sorrentino for providing assistance for X-ray data collection at IBB-CNR, Naples, Italy.

Notes and references

[a] *Dipartimento di Chimica e Biologia, Università degli Studi di Salerno,via Giovanni Paolo II, 132, I-84084 Fisciano, Italy. Fax: +39 089 969603; Tel: +39 089 969586; E-mail: ctedesco@unisa.it*

[b] *Nano_MATES Research Center, Università degli Studi di Salerno, I-84084 Fisciano, Italy*

† Electronic Supplementary Information (ESI) available: crystallographic data in CIF format for compound **5** CCDC 971028. See DOI: 10.1039/b000000x/

‡ Crystal data for **5**: Formula: $C_{36}H_{36}N_4O_4$, FW= 588.69, orthorhombic, space group *Pbca*, Z = 4, *a* = 10.899(3) Å, *b* = 10.055(3) Å, *c* = 27.255(7) Å, *V* = 2986.9(14) Å^3, D_x = 1.309 gcm^{-3}, μ_{calc} = 0.692 mm^{-1}, *F*(000) = 1248.0. Final disagreement indices: $R1 = 0.059$ for 1985 reflections with $I > 2\sigma_I$, $_wR2 = 0.22$ for 2253 reflections.

1 (a) S. Lee, C.-H. Chen, A. and H. Flood, *Nature Chem.,* 2013, **5**, 704–710; (b) M. Xue, Y. Yang, X. Chi, Z. B. Zhang and F. H. Huang, *Acc. Chem. Res.*, 2012, **45**, 1294–1308; (c) E. Marsault and M. L. Peterson, *J. Med. Chem.*, 2011, **54**, 1961–2004; (d) Y. Chen and Y. Liu, *Chem. Soc. Rev*.2010, **39**, 495–505; (e) E. M. Driggers, S. P. Hale, J. Lee and N. K. Terrett, *Nat. Rev. Drug Discov.,* 2008, **7**, 608–624; (f) S. J. Dalgarno, P. K. Thallapally, L. J. Barbour and J. L. Atwood, *Chem. Soc. Rev*., 2007, **36**, 236–245; (g) L. A. Wessjohann, E. Ruijter, D. Garcia-Rivera and W. Brandt, *Mol. Diver*., 2005, **9**, 171–186; (h) S. E. Gibson and C. Lecci, *Angew. Chem. Int. Ed.*, 2006, **45**, 1364–1377; (i) G. W. Gokel, W. M. Leevy and M. E. Weber, *Chem. Rev.*, 2004, **104**, 2723–2750; (l) L. R. MacGillivray and J. L. Atwood, *Nature*, 1997, **389**, 469–472.

2 (a) R. N. Zuckermann, *Pept. Sci.*, 2011, **96**, 545–555; (b) R. N. Zuckermann, J. M. Kerr, S. B. H. Kent and W. H. Moos, *J. Am. Chem. Soc.* 1992, **114**, 10646–10647.

3 J. Sun and R. N. Zuckermann, *ACS Nano*, 2013, **7**, 4715–4732.

4 (a) J. A. Crapster, I. A. Guzei and H. E. Blackwell, *Angew. Chem. Int. Ed.*, 2013, **52**, 5079–5084; (b) J. R. Stringer, J. A. Crapster, I. A. Guzei and H. E. Blackwell, *J. Am. Chem. Soc.* 2011, **133**, 15559–15567; (c) S. A. Fowler and H. E. Blackwell, *Org. Biomol. Chem.,* 2009, **7**, 1508–1524; (d) B. Yoo and K. Kirshenbaum, *Curr. Opin. Chem. Biol.*, 2008, **12**, 714–721; (e) C. W. Wu, K. Kirshenbaum, T. J. Sanborn, J. A. Patch, K. Huang, K. A. Dill, R. N. Zuckermann and A. E. Barron, *J. Am. Chem. Soc.*, 2003, **125**, 13525–13530.

5 (a) B. Yoo, S. B. Y. Shin, M. L. Huang and K. Kirshenbaum, *Chem. Eur. J.*, 2010, **16**, 5528–5537; (b) S. B. Y. Shin, B. Yoo, L. J. Todaro and K. Kirshenbaum, *J. Am. Chem. Soc.*, 2007, **129**, 3218–3225.

6 C. De Cola, S. Licen, D. Comegna, E. Cafaro, G. Bifulco, I. Izzo, P. Tecilla and F. De Riccardis, *Org. Biomol. Chem.*, 2009, 7, 2851–2854.

7 (a) M. L. Huang, M. A. Benson, S. B. Y. Shin, V. J. Torres and K. Kirshenbaum *Eur. J. Org. Chem.* 2013, 3560–3566; (b) M. L. Huang, S. B. Y. Shin, M. A. Benson, V. J. Torres and K. Kirshenbaum, *ChemMedChem*, 2012, **7**, 114–122; (c) K. Kirshenbaum, S. B. Shin, "Peptoid Oligomers, Their Preparation, Pharmaceutical Compositions, and Their Use in Treatment and Prevention of Bacterial, Viral, and Fungal Infections", PCT Intl. Appl. WO 2010098843 A2 20100902, 2010; (d) D. Comegna, M. Benincasa, R. Gennaro, I. Izzo and F. De Riccardis, *Bioorg. Med. Chem.*, 2010, **18**, 2010–2018.

8 P. M. Levine, K. Imberg, M. J. Garabedian and K. Kirshenbaum, J. *Am. Chem. Soc.,* 2012, **134**, 6912−6915.

9 J. Seo, B-C. Lee and R. N. Zuckermann, *Comprehensive Biomaterials,* 2011, **2**, 53–76.

10 (a) F. De Riccardis, C. De Cola, G. Fiorillo, A. Meli, S. Aime, E. Gianolio and I. Izzo, *Org. Biomol. Chem.*, 2014, **12**, 424–431; (b) G. Della Sala, B. Nardone, F. De Riccardis and I. Izzo, *Org. Biomol. Chem.*, 2013, **11**, 726–731.

11 (a) I. Izzo, C. De Cola and F. De Riccardis, *Heterocycles*, 2011, **82**, 981–1006; (b) D. Comegna and F. De Riccardis, *Org. Lett.*, 2009, **11**, 3898–3901; (c) J. M. Holub, H. Jang and K. Kirshenbaum, *Org. Lett.*, 2007, **9**, 3275–3278; (d) J. Dale and K. Titlestad, *Chem. Commun.*, 1969, 656–659.

12 P. Groth, *Acta Chem. Scand.*, 1970, **24**, 780–790.

13 N. Maulucci, I. Izzo, G. Bifulco, A. Aliberti, C. De Cola, D. Comegna, C. Gaeta, A. Napolitano, C. Pizza, C. Tedesco, D. Flot and F. De Riccardis, *Chem. Commun*., 2008, 3927–3929.

14 S. B. L. Vollrath, C. Hu, S. Bräse and K. Kirshenbaum, *Chem. Commun.*, 2013, **49**, 2317–2319.

15 I. Izzo, G. Ianniello, C. De Cola, B. Nardone, L. Erra, G. Vaughan, C. Tedesco and F. De Riccardis, *Org. Lett.*, 2013, **15**, 598–601.

16 α-cyclic peptoids containing proline residues have not been included in this survey due to the presence of a stereogenic centre in the peptoid backbone.

17 a) M. Nishio, Y. Umezawa, K. Honda, S. Tsuboyama and H. Suezawa, *CrystEngComm*, 2009, **11** 1757–1788; b) M. Nishio, *CrystEngComm*, 2004, 6, 130–158; c) M. Nishio, M., Hirota and Y. Umezawa, *The CH/pi Interaction. Evidence, Nature, and Consequences*, Wiley-VCH, Weinheim, Germany, 1998; d) G. R. Desiraju, *Acc. Chem. Res.*, 1991, **24**, 290–296.

18 *The Importance of Pi-Interactions in Crystal Engineering: Frontiers in Crystal Engineering* Eds. E. R. T. Tiekinkand and J. Zukerman-Schpector, John Wiley & Sons Ltd, Chichester, UK, 2012; b) J. D. Dunitz and A. Gavezzotti, *Chem. Soc. Rev.,* 2009, **38**, 2622–2633; c) G. R. Desiraju and T. Steiner, *The Weak Hydrogen Bond in Structural Chemistry and Biology*, Oxford Science Publication, Oxford, 1999.

19 (a) J. J. McKinnon, D. Jayatilaka and M. A. Spackman, *Chem. Commun*., 2007, 3814; (b) J. J. McKinnon, M. A. Spackman and A. S. Mitchell, *Acta Crystallogr., Sect. B: Struct. Sci*., 2004, **60**, 627–668; (c) M. A. Spackman and J. J. McKinnon, *CrystEngComm*, 2002, **4**, 378–392.

20 P. Groth, *Acta Chem. Scand. A* , 1976, **30**, 838–840.

21 H. Hioki, H. Kinami, A. Yoshida, A. Kojima, M. Kodama, S. Takaoka, K. Uedab and T. Katsu, *Tetr. Lett*., 2004, **45**, 1091–1094.

22 (a) C. Tedesco, L. Gregoli, I. Immediata, E. Gavuzzo and P. Neri, *Cryst. Growth Des.* 2008, **8**, 3700–3705; (b) J. L. Atwood, L. J. Barbour, A. Jerga and B. L. Schottel, *Science*, 2002, **298**, 1000–1002.

23 (a) D. T. Bong, T. D. Clark, J. R. Granja and M. R. Ghadiri, *Angew. Chem. Int. Ed.*, 2001, **40**, 988–1011; (b) J. D. Hartgerink, J. R. Granja, R. A. Milligan and M. R. Ghadiri, *J. Am. Chem. Soc.*, 1996, **118**, 43–50; (c) M. R. Ghadiri, J. R. Granja, R. A. Milligan, R. E. McRee and N. Khazanovich, *Nature*, 1993, **366**, 324–327.

24 $\chi 1$ angles are defined as C(i–1)—N—(N–Cα)—(N–Cβ) according to G. L. Butterfoss, D. Renfrew, B. Kuhlman, K. Kirshenbaum and R. Bonneau, *J. Am. Chem. Soc.*, 2009, **131**, 16798–16807.

25 P. Groth, *Acta Chem. Scand.*, 1973, **27**, 3419–3426.

26 P. Groth, *Acta Chem.Scand. A*, 1977, **31**, 838–840.

27 N. H. Shah, G. L. Butterfoss, K. Nguyen, B. Yoo, R. Bonneau, D. L. Rabenstein and K. Kirshenbaum, *J. Am. Chem. Soc.*, 2008, **130**, 16622–16632.

28 B. Paul, G. L. Butterfoss, M. G. Boswell, M. L. Huang, R. Bonneau, C. Wolf and K. Kirshenbaum, *Org. Lett.*, 2012, **14**, 926–929.

29 F. Grepioni, G. Cojazzi, S. M. Draper, N. Scully and D. Braga, O*rganometallics*, 1998, **17**, 296–307.

30 P. Groth, *Acta Chem. Scand. A*, 1975, **29**, 38–44.

31 a) P. Groth, *Acta Chem. Scand.*, 1973, **27**, 3217–3226; b) K. Titlestad, P. Roth, J. Dale and M. Y. Ali, *J.C.S. Chem. Comm.,* 1973, 346–347.

32 G. L. Butterfoss, B. Yoo, J. N. Jaworski, I. Chorny, K. A. Dill, R. N. Zuckermann, R. Bonneau, K. Kirshenbaum and V. A. Voelz, *Proc. Natl. Acad. Sci. U.S.A*., 2012, **109**, 14320–14325.

33 P. Groth, *Acta Chem. Scand. A*, 1976, **30**, 840–842.

34 CrystalClear, Crystal Structure Analysis Package, Rigaku-Molecular Structure Corp.

35 M. C. Burla, M. Camalli, B. Carrozzini, G. Cascarano, C. Giacovazzo, G. Polidori and R. Spagna, *J. Appl. Cryst.*, 2001, **34**, 523–526.

36 G. M. Sheldrick, *Acta Cryst. A*, 2008, **64**, 112–122.

37 C. F. Macrae, I. J. Bruno, J. A. Chisholm, P. R. Edgington, P. McCabe, E. Pidcock, L. Rodriguez-Monge, R. Taylor, J. van de Streek and P. A. Wood, *J. Appl. Cryst.*, 2008, **41**, 466–470.

38 S. K. Wolff, D. J. Grimwood, J. J. McKinnon, M. J. Turner, D. Jayatilaka and M. A. Spackman, CrystalExplorer (Version 3.1), University of Western Australia, 2013.

39 F. H. Allen, O. Kennard, D. G. Watson, L. Brammer, A. G. Orpen and R. Taylor, *International Tables for Crystallography*, pp 685–706, Ed. A. J. C. Wilson, Kluwer Academic, Dordrecht, 1995.

